CHARACTERIZATION OF SMALL SCALE HETEROGENEITY FOR PREDICTION OF ACID FRACTURE PERFORMANCE

A Thesis

by

CASSANDRA VONNE BEATTY

Submitted to the Office of Graduate Studies of
Texas A&M University
in partial fulfillment of the requirements for the degree of

MASTER OF SCIENCE

August 2010

Major Subject: Petroleum Engineering

Characterization of Small Scale Heterogeneity for Prediction of Acid Fracture Performance

CHARACTERIZATION OF SMALL SCALE HETEROGENEITY FOR PREDICTION OF ACID FRACTURE PERFORMANCE

A Thesis

by

CASSANDRA VONNE BEATTY

Submitted to the Office of Graduate Studies of
Texas A&M University
in partial fulfillment of the requirements for the degree of

MASTER OF SCIENCE

Approved by:

Chair of Committee,	A. Daniel Hill
Committee Members,	Ding Zhu
	Wayne M. Ahr
Head of Department,	Stephen A. Holditch

August 2010

Major Subject: Petroleum Engineering

ABSTRACT

Characterization of Small Scale Heterogeneity for Prediction of Acid Fracture Performance. (August 2010)

Cassandra Vonne Beatty, B.S., Cornell University

Chair of Advisory Committee: Dr. A. Daniel Hill

Recently developed models of the acid fracturing process have shown that the differential etching necessary to create lasting fracture conductivity is caused by the heterogeneous distributions of permeability and mineralogy along the fracture faces. To predict the conductivity that can be created by acid in a particular formation, the models require information about these formation properties. This research aims to quantify correlation lengths using a geostatistical description of small scale heterogeneity to ascertain the distribution of permeability and mineralogy in a carbonate formation. The correlation length parameters are a first step in being able to couple acid transport and rock dissolution models at reservoir scale with a model of fracture conductivity based on channels and roughness features caused by small scale heterogeneity.

Geostatistical parameters of small scale heterogeneity affecting wells in the Hugoton Field are developed. Data leading to their derivation are obtained from a combination of well logs and cores. The permeability of slabbed core is measured to yield vertical correlation length. Well logs are used to estimate permeability via an empirical relationship between core plug permeability and well log data for calculation

of horizontal correlation length. A fracture simulator computes the acid etched fracture width for known treatment conditions. The resulting geostatistical parameters and acid etched width are used to predict acid fracture performance for a well in the Hugoton Field. Application of new model conductivity correlations results in a unique prediction for the acid fracture case study that differs from the industry standard.

Improvements in low cost stimulation treatments such as acid fracturing are the key to revitalizing production in mature carbonate reservoirs like the Hugoton Field. Planning and development of new wells in any carbonate formation necessarily must consider acid fracturing as a production stimulation technique. Reliable models that accurately predict acid fracture conductivity can be used to make an informed investment decision.

DEDICATION

Dedicated to the men who love freedom and who take those first steps down new roads armed with nothing but their own vision.

ACKNOWLEDGEMENTS

Thank you to Dr. Hill and Dr. Zhu for taking a chance on a young woman from Oregon. Thank you to Richard Sullivan for his patience and support of research. Thank you to Jianye Mou for doing the hard work before me so that I may continue with this thesis and Jiayao Deng for carrying on with this work. Thank you, Dr. Ahr, for meeting me on the bridge between engineering and geology, sharing insight, experience, and good nature. Thank you to my partner, Larry Oeth, for his unflagging encouragement, love, humor, and culinary skill, which carried me through this degree and thesis.

NOMENCLATURE

API	American Petroleum Institute
SGeMS	Stanford Geostatistical Modeling Software
SPE	Society of Petroleum Engineers
$f_{\text{limestone}}$	fraction of limestone on the fracture face
k	permeability, md
$\bar{k}$	average permeability, md
k_{90}	permeability 90º from horizontal permeability in the horizontal plane, md
k_{air}	permeability to air, md
k_H	horizontal permeability, md
$\left(k_f w\right)_0$	acid fracture conductivity at zero closure stress, md-ft
$\gamma(h)$	variance with respect to separation distance
h	separation distance
λ	correlation length, ft
$\lambda_{D,x}$	normalized correlation length in the x direction
$\lambda_{D,z}$	normalized correlation length in the z direction
λ_x	correlation length in the x direction, ft
λ_z	correlation length in the z direction, ft

N	number of data pairs per variogram calculation
σ_D	dimensionless standard deviation of the natural log of permeability
$\overline{w}$	average acid fracture width, in
w_i	ideal fracture width, in
z_i	data used in variogram calculation at position i
z_{i+h}	data used in variogram calculation at position $i+h$

TABLE OF CONTENTS

Page

LIST OF FIGURES

FIGURE Page

FIGURE Page

LIST OF TABLES

1. INTRODUCTION

1.1 Acid Fracture Conductivity Prediction

Acid fracturing is a well stimulation technology for carbonate reservoirs that requires uneven dissolution of the rock fracture face (Ruffet et al., 1997; Malagon et al., 2006; Antelo et al., 2009; Pournik et al., 2009). In the acid fracturing process, a fracture is created with hydraulic pressure and the acid dissolves the rock along the faces of the fracture. At the end of the fracturing process, the high pressure in the fracture is relieved and earth stresses force the fracture to close. Differential etching from uneven dissolution of the fracture face is expected to have occurred. As the fracture closes, parts of the fracture will remain open allowing oil or gas to flow to the well. Thus, the acid fracturing process requires heterogeneity to work. If the rock were uniform, the etching would be uniform and the fracture would close, leaving no lasting conductivity. Efficient use of this technique depends upon prediction of acid fracture conductivity at reservoir scale using a model which incorporates the effects of small scale sedimentary rock heterogeneity, which provide the differential etching required for retention of fracture conductivity.

No conductivity correlation accurately predicts acid fracture conductivity at reservoir scale, despite the theoretical and experimental work on the subject (Nierode and Kruk, 1973; Gong et al., 1998; Pournik et al., 2009; Mou et al., 2010). The most widely used correlation was developed by Nierode and Kruk (1973) and requires

---

This thesis follows the style of *SPE Journal.*

experimental data on acid fracture conductivity from a laboratory test. The resulting conductivity is based on the volume of rock dissolved and the rock mechanical strength. No parameter in the correlation accounts for rock heterogeneity, and the experiments use samples that are too small to capture the heterogeneity relevant to the overall acid fracturing process. Correlations since have attempted to include parameters that quantify the fracture surface roughness, but these correlations employ idealized analytical solutions that generalize the mechanism of conductivity generation and are based on small laboratory rock samples unrepresentative of the overall acid fracture (Gangi, 1978; Walsh, 1981; Gong et al., 1998; Pournik et al., 2009).

Acid fracture conductivity is dependent on surface etching patterns, which are determined by the distribution of permeability and mineralogy along the fracture face (Malagon et al., 2006; Deng et al., 2009, Mou et al., 2009, Pournik et al., 2009). An accurate prediction of acid fracture conductivity necessitates the detailed description of the acid etching profile on each fracture surface, which depends on acid transport in the fracture, leakoff due to local permeability, and acid/rock reactions (Malagon et al., 2006; Mou et al., 2009). Mou et al. (2009) have developed an intermediate scale model using grid blocks 10 feet by 10 feet to predict the pressure field, flow field, acid concentration profile, and fracture surface profile as a function of acid injection volume. In the model, the distributions of permeability and mineralogy along the fracture face are geostatistically generated as the initial fracture conditions. By changing these statistical parameters, different kinds of mineralogy and permeability distributions can serve as inputs to the model (**Fig. 1.1**).

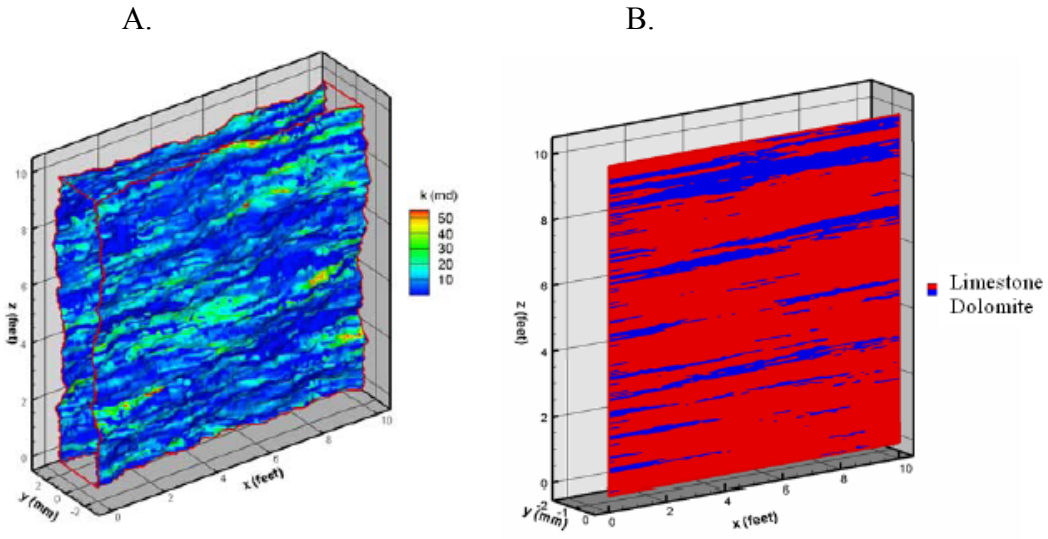

Fig. 1.1—Example of the A.) permeability and B.) mineralogy distribution along fracture surfaces (Mou, 2009).

The model outputs the fracture surface etching profiles as a function of acid contact time, and the fracture width distribution can be obtained from the profiles (**Fig. 1.2**).

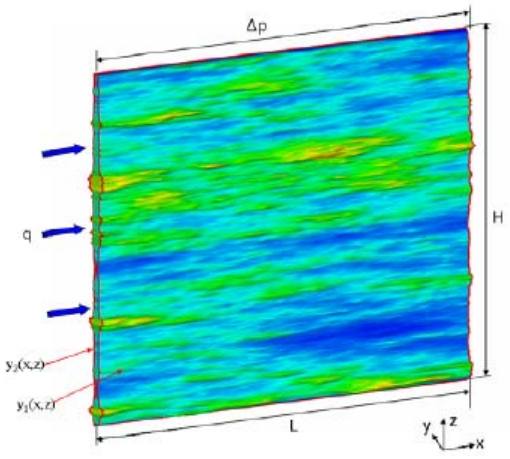

Fig. 1.2—Acid etched fracture faces just touching at zero closure stress (Mou, 2009).

The model then calculates the fracture conductivity by solving for the flow rate within the irregular fracture domain given a fixed pressure drop. By analyzing the relationship between the fracture conductivity created and statistical properties of the permeability and mineralogy distributions, Mou et al. (2010) developed new acid fracture conductivity correlations at zero closure stress. These correlations are case specific:

1.) Permeability distribution dominant case

This case is appropriate given a:

- High total leakoff coefficient, which is defined as being higher than $0.004\ \text{ft}/\sqrt{\text{min}}$ under typical fracturing conditions, or
- Medium leakoff coefficient (approximately equal to $0.001\ \text{ft}/\sqrt{\text{min}}$) with a uniform mineralogy distribution (100% limestone or 100% dolomite).

The conductivity correlation is:

$$\left(k_f w\right)_0 = 4.48\times10^9\,\overline{w}^3\left[1+\left(1.82*erf(3.25*(\lambda_{D,x}-0.12))\right.\right.$$

$$\left.\left.-1.31*erf(6.71*(\lambda_{D,z}-0.03))\right)\sqrt{(e^{\sigma_D}-1)}\right] \quad \textbf{(1.1)}$$

The average width, $\overline{w}$, is defined for a high leakoff coefficient:

$$\overline{w} = 0.56*erf(0.8*\sigma_D)w_i^{0.83} \quad \textbf{(1.2)}$$

Alternatively, for a medium leakoff coefficient and uniform mineralogy, the average width, $\overline{w}$, is defined:

$$\overline{w} = 0.2*erf(0.78*\sigma_D)w_i^{0.81} \quad \textbf{(1.3)}$$

2.) Mineralogy distribution dominant case

This case is appropriate given a small leakoff coefficient, which is a leakoff coefficient less than 0.0004 ft/$\sqrt{\text{min}}$ under typical fracturing conditions. The conductivity correlation is:

$$\left(k_f w\right)_0 = 4.48\times10^9\,\overline{w}^3\left[1+2.97*\left(1\text{-}f_{\text{limestone}}\right)^{2.02}\right] \quad \textbf{(1.4)}$$

The average width, $\overline{w}$, is defined for this case:

$$\overline{w} = 0.13*(f_{\text{limestone}})^{0.56} w_i^{0.84} \quad \textbf{(1.5)}$$

where $f_{\text{limestone}}$ is the limestone fraction along the fracture face.

3.) Competing effect of permeability and mineralogy distributions case

This case is appropriate given a leakoff coefficient that is around 0.001 ft/$\sqrt{\text{min}}$. The conductivity correlation is:

$$\left(wk_f\right)_0 = 4.48\times10^9\,\overline{w}^3\left[1+0.2+\left(1.0*erf(5.0*(\lambda_{D,x}-0.12))\right.\right.$$

$$\left.\left.-0.6*erf(3.5*(\lambda_{D,z}-0.03))\right)\sqrt{(e^{\sigma_D}-1)}\right] \quad \textbf{(1.6)}$$

The average width, $\overline{w}$, is defined for this case:

$$\overline{w} = \left(0.1*(f_{\text{limestone}})^{0.43}+0.14*\sigma_D\right)w_i^{0.84} \quad \textbf{(1.7)}$$

The conductivity at zero closure stress, $\left(wk_f\right)_0$, is in md-ft in these correlations, and the average width, $\overline{w}$, is in inches. The average fracture width, $\overline{w}$, must be calculated for each of the above cases, which requires detailed knowledge of the etched fracture

surface profiles. $\overline{w}$ is expressed as a function of the ideal fracture with, w_i. This width is equal to the dissolved rock volume divided by the fracture rock surface area, $w_i = \frac{\text{dissolved rock volume}}{(1-\phi)*\text{area}}$.

The Mou et al. (2010) conductivity correlations contain statistical parameters that quantify the distribution of permeability and mineralogy across the fracture face. The dimensionless term $\lambda_{D,x}$ is a ratio of permeability correlation length in the horizontal direction to the grid block length (grid blocks are 10 feet by 10 feet in area) used in the Mou (2009) model, $\lambda_{D,x} = \lambda_x/10$. $\lambda_{D,z}$ is also a ratio of permeability correlation length to grid block size, but this parameter is specific to the vertical direction ($\lambda_{D,z} = \lambda_z/10$). These parameters quantify how strongly the permeability trends in a lateral and vertical direction. σ_D is a dimensionless standard deviation parameter, equal to $\sigma_D = \sigma(\ln(k))/\ln(\bar{k})$. $\sigma(\ln(k))$ is the standard deviation of the natural logarithm of permeability ($\ln(k)$), and $\bar{k}$ is the average permeability. The σ_D term is essentially a coefficient of variation parameter that measures the dispersion of the permeability distribution.

The permeability distribution is quantified by correlation length, λ, which is defined using the variogram model. A variogram is a graphical tool that plots variability within a dataset with respect to location of the data (**Fig. 1.3**).

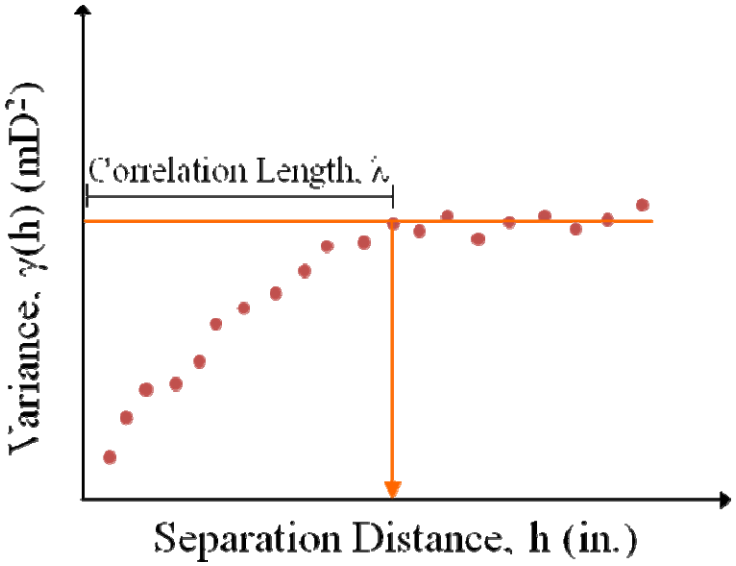

Fig. 1.3—Sample variogram.

The equation that describes the plot above is as follows:

$$\gamma(h) = \frac{1}{2N}\Sigma\left(z_i - z_{i+h}\right)^2 \quad \text{.....(1.8)}$$

$\gamma(h)$ is the variance, N is the number of data pairs at separation distance h, z_i are individual data points, and z_{i+h} are individual data points located h distance away from z_i. Each point on the variogram represents the relationship between data pairs from the original dataset separated by distance h. The permeability measurements display decreasing similarity (quantified as an increase in variance) as the distance between data points is increased, eventually reaching a plateau. The distance at which this occurs is known as the correlation length, λ (Isaaks and Srivastava, 1989). The determination of the vertical (z-axis) and horizontal (x-axis) correlation lengths requires numerous data points separated at a distance that allows the typical variogram shape and resulting

correlation length to be readily observed. The dimensionless standard deviation parameter, σ_D , can also be calculated from this dataset.

1.2 Background for Case Study

The Hugoton Field underlies much of southwest Kansas, passes through the panhandle of Oklahoma, and extends into Texas (**Fig. 1.4**).

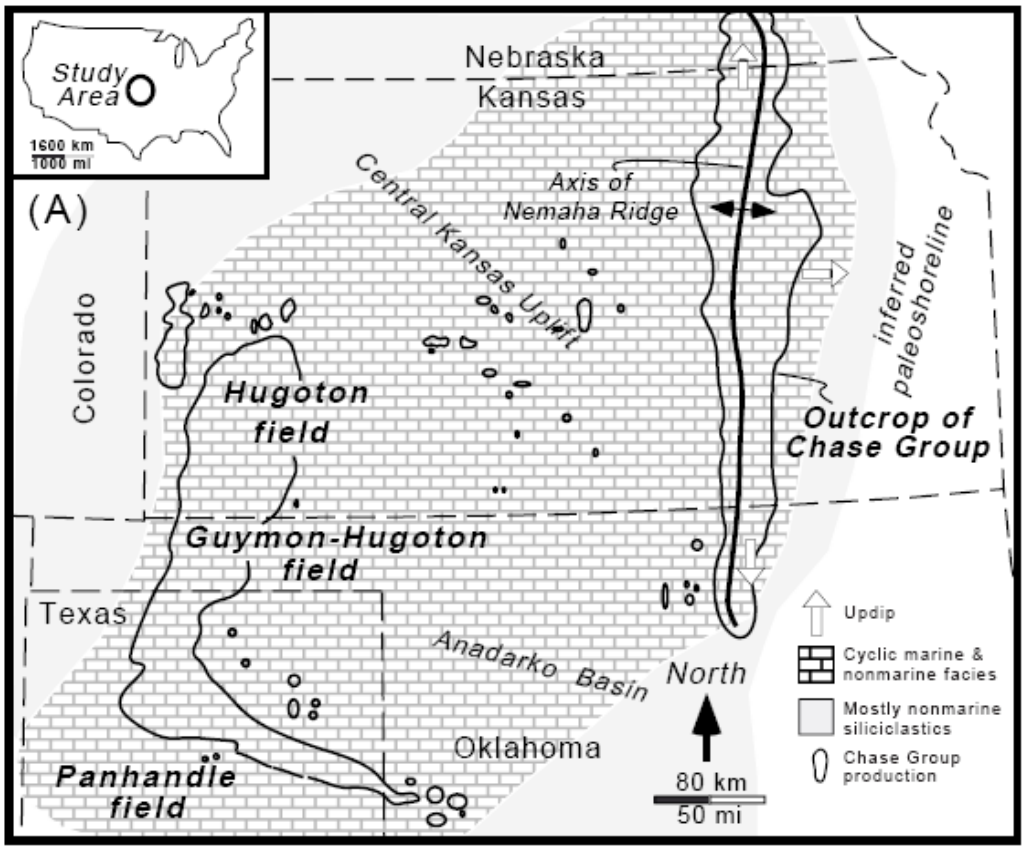

Fig. 1.4—The location and extent of the Hugoton Field (Mazzullo, 1998).

The field contains a large, domestic source of natural gas with an estimated 75 Tcf ultimate recovery, representing the largest conventional gas field in North America (Dubois et al., 2006). Approximately 34 Tcf of dry gas have already been recovered over a 70-year period from the Kansas and Oklahoma portion of the field (Dubois et al., 2006). Estimates of remaining reserves for two of the most prolific counties, Grant and Stevens County in Kansas, approach 8 Tcf and the infrastructure for additional recovery is in place (Dubois et al., 2006). The Hugoton Field has been in active production since the 1920s, but further recovery has been prevented to date because remaining reserves are in low permeability, differentially depleted carbonate members (Lisigurski and Rowe, 2006).

The productive members of the Hugoton field are contained within the Chase Group and Council Grove Group (**Fig. 1.5**).

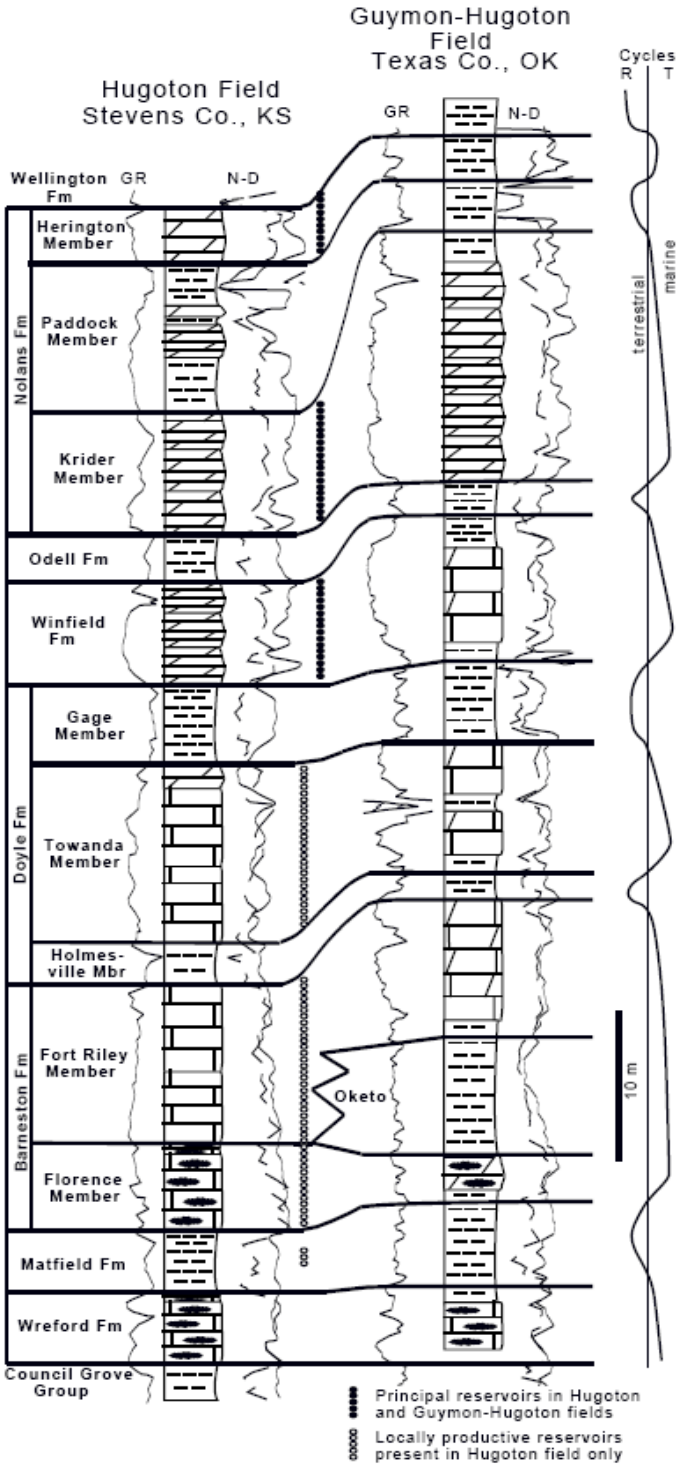

Fig. 1.5—The Chase Group in the Hugoton Field of Kansas (Mazzullo, 1998).

Historically, production has occurred from the top three carbonate members of the Chase Group, but all ten major members of the Chase and all of the Council Grove Group members contain gas (LeFever and Schaefer, 1947; Ebbs et al., 1990; Dubois et al., 2006). The layered reservoir system consists of marine-continental cycles, comprising thin-bedded, marine carbonate mudstone to grainstone and siltstones to very fine sandstone (Siemers and Ahr, 1990; Dubois et al., 2006). The primary pay zones (carbonate members) are separated by eolian and/or sabkha red beds, which have low reservoir quality (Siemers and Ahr, 1990; Dubois et al., 2006). The layering represents the cyclic depositional environment of a marine shelf, changing in response to rapid sea level fluctuation (Siemers and Ahr, 1990; Dubois et al., 2006). The important reservoir lithofacies are laterally extensive as the marine carbonates are separated by laterally continuous continental siltstone with poor vertical transmissibility (Siemers and Ahr, 1990; Dubois et al., 2006). Due to the updip changes in lithofacies and petrophysical properties associated with these changes, the Hugoton Field is a classic example of a giant stratigraphic trap as the marine carbonate intervals thin or pinch-out at the field's western updip margin with the relationship being nearly reciprocal basinward (Dubois et al., 2006).

These members must be stimulated to produce commercial quantities of gas (Lisigurski and Rowe, 2006). Early completions were commonly open hole with a slotted liner followed by a large acid treatment, and after 1960 typical completions commonly involved casing, perforation, acidizing, and a large hydraulic sand fracture treatment (Dubois et al., 2006). The key to unlocking the huge remaining reserves may

be in the application of low cost hydraulic fracturing treatments. Acid fracturing can be many times cheaper than a propped fracture treatment in carbonate reservoirs. Improvements in acid fracturing technology may revitalize production from the Hugoton Field as well as other carbonate reservoirs.

1.3 Problem Description

Efficient use of acid fracturing as a stimulation technique depends upon prediction of acid fracture conductivity at reservoir scale using a model which incorporates the effects of small scale sedimentary rock heterogeneity. Most commonly used conductivity correlations of the acid fracturing process are based on etching in samples that are on the order of inches and tested in the lab. In reality, acid fractures may extend hundreds of feet in height and length and fracture conductivity is dependent on non-uniform etching of the fracture faces, which requires knowledge of the variation of formation properties across the fracture. The goal of this research is to develop a mathematical description of the small scale carbonate rock heterogeneity that drives the treatment process and use it to predict acid fracture performance at reservoir scale for a specific well in the Hugoton Field. The Mou et al. (2010) conductivity correlations will be used as these are the only conductivity correlations that incorporate parameters representative of differential etching, which is the mechanism that creates acid fracture conductivity.

1.4 Objectives of Research

This research has two main objectives:

1. Identify, collect, and analyze the data required to quantify small scale carbonate heterogeneity. A challenge in understanding and quantifying the heterogeneity at the acid fracture scale is lack of data. There is a need for data that can characterize rock at a scale appropriate for an acid fracture and particularly in the horizontal direction. Using this data, geostatistical parameters required by the Mou et al. (2010) conductivity correlations will be generated (specifically λ_x, λ_z, and σ_D).
2. Predict the conductivity of an acid fractured well in the Hugoton Field using the new correlations developed by Mou et al. (2010). For a specific case in the Hugoton Field, permeability has been directly measured with a probe permeameter along slabbed vertical segments of core and a lateral well log has been used to estimate permeability via an empirical relationship between core plug permeability and well log data. Analysis of the permeability dataset has yielded the geostatistical parameters required by the Mou et al. (2010) correlations. Operator supplied data has been input to a fracture simulator (E-StimPlan 3D 6.00 developed by NSI Technologies) for output of the acid etched fracture width, w_i. The acid etched fracture width in combination with the derived geostatistical parameters have been used in the Mou et al. (2010) conductivity correlations to produce a map of conductivity across the fracture,

calculate total fracture conductivity, and estimate the impact of the acid fracture on well performance.

2. SOURCES OF DATA FOR GEOSTATISTICAL QUANTIFICATION

2.1 Introduction

Sedimentary rocks exhibit heterogeneity at many scales (Ahr, 2008). Much research has been conducted to describe heterogeneity at the reservoir scale for application to reservoir simulation. However, many underground processes depend on heterogeneity at a smaller scale. The success of production and injection procedures depends on understanding the role of heterogeneity at very small scales.

A challenge in understanding and quantifying the heterogeneity at a small scale relevant to acid fracture performance is lack of data. Reservoir scale geology is observed via seismic surveys, outcrops, and logging data from wells that may be miles apart. Slabbed cores from individual wells provide qualitative geological information and quantitative petrophysical data. Core plugs can be used for correlation of logging data to reservoir petrophysical properties and for defining facies and petrophysical rock types across a field. However, core sampling is typically confined to the vertical section of wells. The same is true for well logs. Production data and tests can refine geologic insight but result in averages for each productive zone, giving little indication of the heterogeneity across a zone. There is a need for data that can characterize rock composition and permeability at a scale appropriate for an acid fracture and particularly in the horizontal direction.

Three sources of data were identified for the case in the Hugoton Field: slabbed core, outcrops, and well log and petrophysical correlation data.

2.2 Slabbed Core Permeability Measurements

Slabbed core from a Hugoton Field well was measured using a portable probe permeameter (**Fig. 2.1**).

Fig. 2.1—Slabbed core with visible alternating continental red bed and gray marine member layers.

The probe permeameter is an unsteady state permeability measurement device. The theory of the device is described in API Recommended Practice 40 (1998) and by Jones (1992). The equipment takes nondestructive permeability measurements using air supplied to a reservoir with a bike pump. A couple of valves allow the operator to supply pressure from the reservoir to the probe tip, and this probe tip is placed against the rock sample face. As the pressure behind the probe tip is spent, the equipment software matches a curve based on the probe tip geometry and pressure decay to predict permeability (**Fig. 2.2**).

Fig. 2.2—Probe permeameter equipment, PPP-250 and Samsung Q1 PC, used to measure permeability to air of slabbed core.

Using well log and geological description information supplied by the operator, the productive members of the Hugoton Chase Group were identified for slabbed core from two wells. Six 10 foot vertical sections of core were measured. Permeability measurements were taken every inch over these approximately 10 foot sections. Seal quality was critical for accurate permeability measurement. Each reading took between a few seconds and one minute, with the permeability to air instantly reported using the accompanying equipment (PPP-250) software.

Noticeable along the slabbed core were sources of heterogeneity that have a significant impact on acid fracture performance (**Fig. 2.3**).

Fig. 2.3—Visible anhydrite nodules in the Krider member.

Other features observed to be contributing to the variation along the productive members include burrows, ripples, laminations, crossbeds, fossils, marine sands (characterizing a shoal environment), skeletal debris, and root mottling. Against a dominant diagenetic dolomite or grainstone, packstone, wackestone, or mudstone depositional fabric, these variations limit significantly the extent of vertical permeability correlation.

2.3 Outcrop Field Work

The Permian age rock that makes up the Hugoton Field outcrops in eastern Kansas (**Figs. 2.4-2.5**).

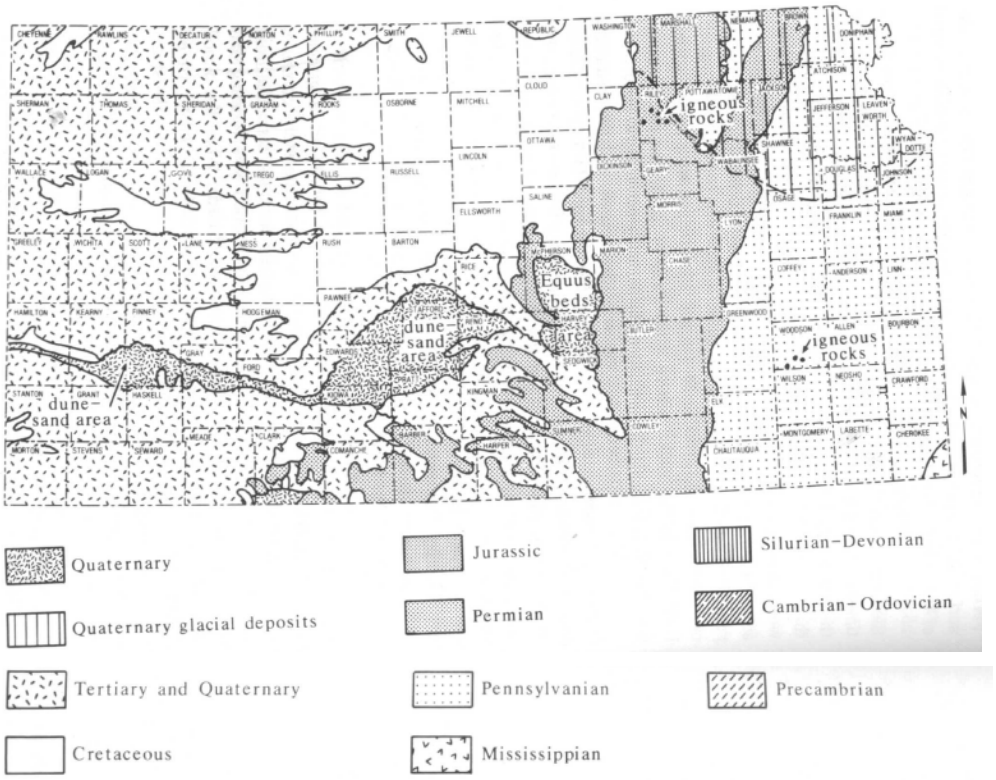

Fig. 2.4—Map of age of surface rock across Kansas (Buchanan and McCauley, 1987).

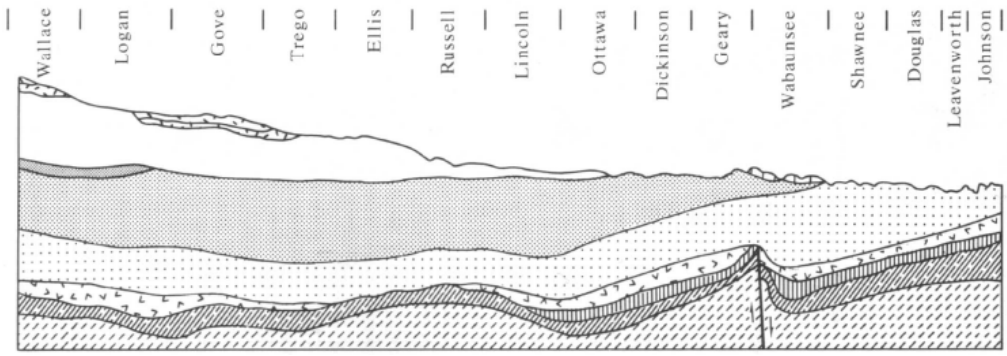

Fig. 2.5—Cross section of Kansas subsurface geology (Buchanan and McCauley, 1987).

The extensive outcrop study done by Mazzullo et al. (1996) and Mazzullo (1999) suggest Geary County and Riley County to contain outcrops suitable for comparison to the subsurface reservoir rock in Stevens County. Two trips were taken to quarry locations near Riley, Kansas. During the first trip, the PPP-250 equipment was used to measure Towanda member outcrop permeability along transects (**Fig. 2.6**).

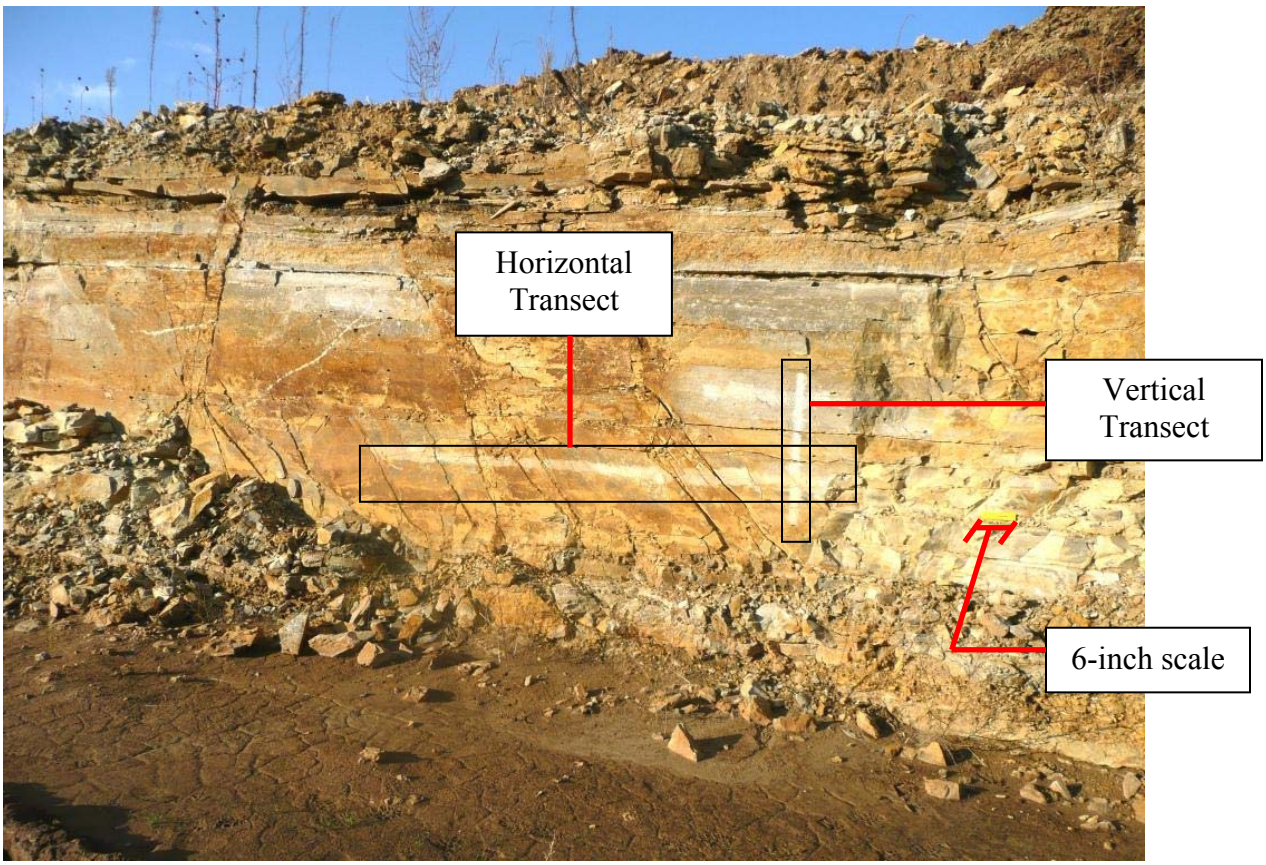

Fig. 2.6—Kansas outcrop and transects for PPP-250 measurements.

The outcrop surface was weathered, uneven, and extremely tough. The rock was too hard to chip away with a rock hammer. Grinding the surface only caused the ground

rock to become embedded firmly in the surface, altering any natural permeability that could be measured with the PPP-250. Samples from the outcrop were also acidized with HCl and cut with a diamond blade cutoff saw. Neither action produced a smooth, unaltered surface for accurate permeability measurement with the PPP-250. Placing Silly Putty around the probe tip did accommodate some surface unevenness, but the weathered or altered exterior rock surface prevented accurate permeability measurement. Other studies, however, have reported success using the PPP-250 to measure outcrop permeability (Goggin et al., 1988; Goggin et al., 1992; Hartkamp-Bakker and Donselaar, 1993; Jennings et al., 1998).

A common technique for measuring the spatial distribution of permeability across a geologic member is to collect core plugs at regular spacing along an analogous outcrop (Tomutsa et al., 1986; Borgia et al., 1997; Pranter et al., 2005). The second trip to the outcrop site prompted coordination with a local coring business. A total of 83 intact, 2 x 1 inch core plugs were obtained from the outcrop face using drills equipped with impregnated diamond core bits (**Fig. 2.7**).

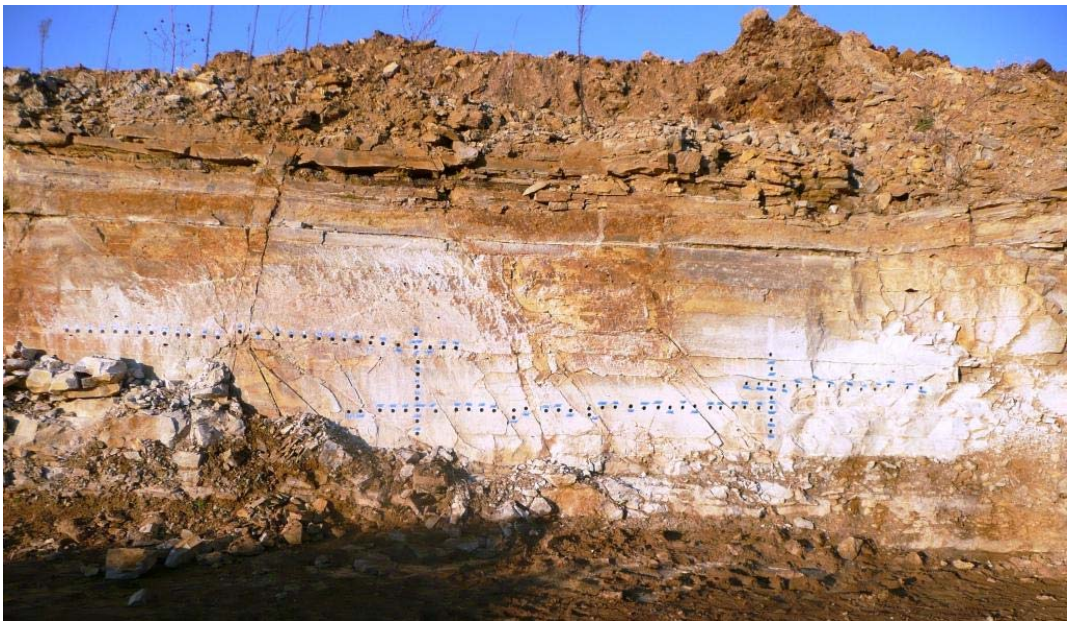

Fig. 2.7—Sample locations along Towanda outcrop in quarry near Riley, KS.

The permeability of each core plug was measured in a standard Hassler sleeve device (API, 1998). No core plug had permeability to air greater than approximately 0.005 md based on the sensitivity of laboratory equipment. The significantly reduced permeability explains the difficulty in using the PPP-250 equipment to measure outcrop permeability, even with low (less than 2 psi) probe back pressure (i.e., the seal quality was poor given the low rock permeability and measurements were beyond the range of the PPP-250). Given how substantially the core plugs differed from the measured slabbed core permeability (average for the Towanda member is approximately 5.7 md), the outcrops were discounted from being analogous to the subsurface reservoir rock with respect to petrophysical properties.

To be truly analogous, outcrops must be of the same age, depositional environment, and diagenetic alteration as the reservoir rock studied (Borgia et al., 1997). The outcrop was highly fractured. Natural fractures have not been observed in the reservoir subsurface (Dubois et al., 2006). Additionally, it is likely the diagenetic alteration experienced by exposed rock of shallow burial is far different than that of the subsurface reservoir rock, which is thousands of feet below the surface. Due to the susceptibility of carbonates to mechanical and chemical change, it is unlikely that outcrops of geologic members more than 200 miles from the subsurface reservoir rock would contain identical petrophysical properties.

2.4 Lateral Log Data and Permeability Correlation

The operator developed a correlation for permeability based on porosity log and core plug permeability data. A relationship between log effective porosity and measured core plug permeability was defined using the V_{clay} (volume fraction of clay) portion from the porosity logs to define log effective porosity. Based on the density of the log readings, this permeability relationship provided estimated permeability data every six inches along the lateral.

3. GEOSTATISTICAL PARAMETERS

3.1 Vertical Correlation Length

The slabbed core permeability measurements served as the basis for definition of the vertical correlation length. For two wells in the Hugoton Field, permeability measurements were taken every inch along approximately 10 foot vertical sections in the Towanda and Fort Riley geologic members. These are the largest geologic members, containing the most remaining gas reserves of any in the Hugoton Field (Dubois et al., 2006). The Fort Riley member is divided into two layers based on depositional environment: a shoal characterizes the Upper Fort Riley and a lagoon environment typifies the Lower Fort Riley.

The permeability data is plotted with respect to depth and a variogram created for each vertical 10 foot section of measured slabbed core. Three sections were measured for two wells, yielding a total of six 10 foot vertical sections. The correlation length that affects acid fracture performance is on the order of inches based on the model created by Mou (2009), which used 10 foot by 10 foot grid blocks in the development of conductivity correlations. Therefore, only the first structure observed in each variogram is modeled using either the spherical, Gaussian, or pure nugget variogram models (Isaaks and Srivastava, 1989). A nugget effect across all the variograms of 5 md^2 is used. Every variogram is a plot of variance, $\gamma(h)$, on the ordinate with respect to separation distance between data pairs, h, on the abscissa. All variograms were prepared using Stanford Geostatistical Modeling Software (Remy et al., 2008).

A highly permeable (k_{air} > 10 md) segment of core exists near the top of the Well 1 Towanda member measured slabbed core section (**Fig. 3.1**).

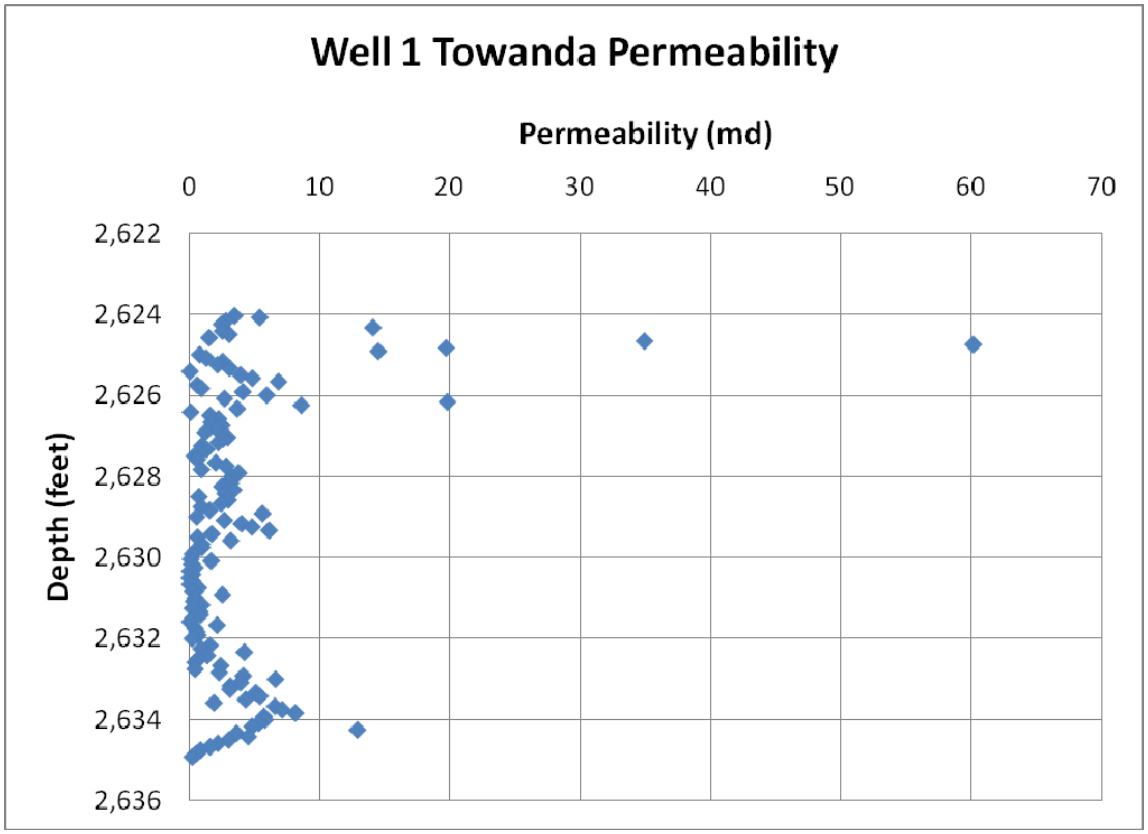

Fig. 3.1—Well 1 Towanda slabbed core permeability.

This produces a hole-effect in the variogram (**Fig. 3.2**), reflecting a local minimum once the maximum variance or sill is reached (Gringarten and Deutsch, 1999).

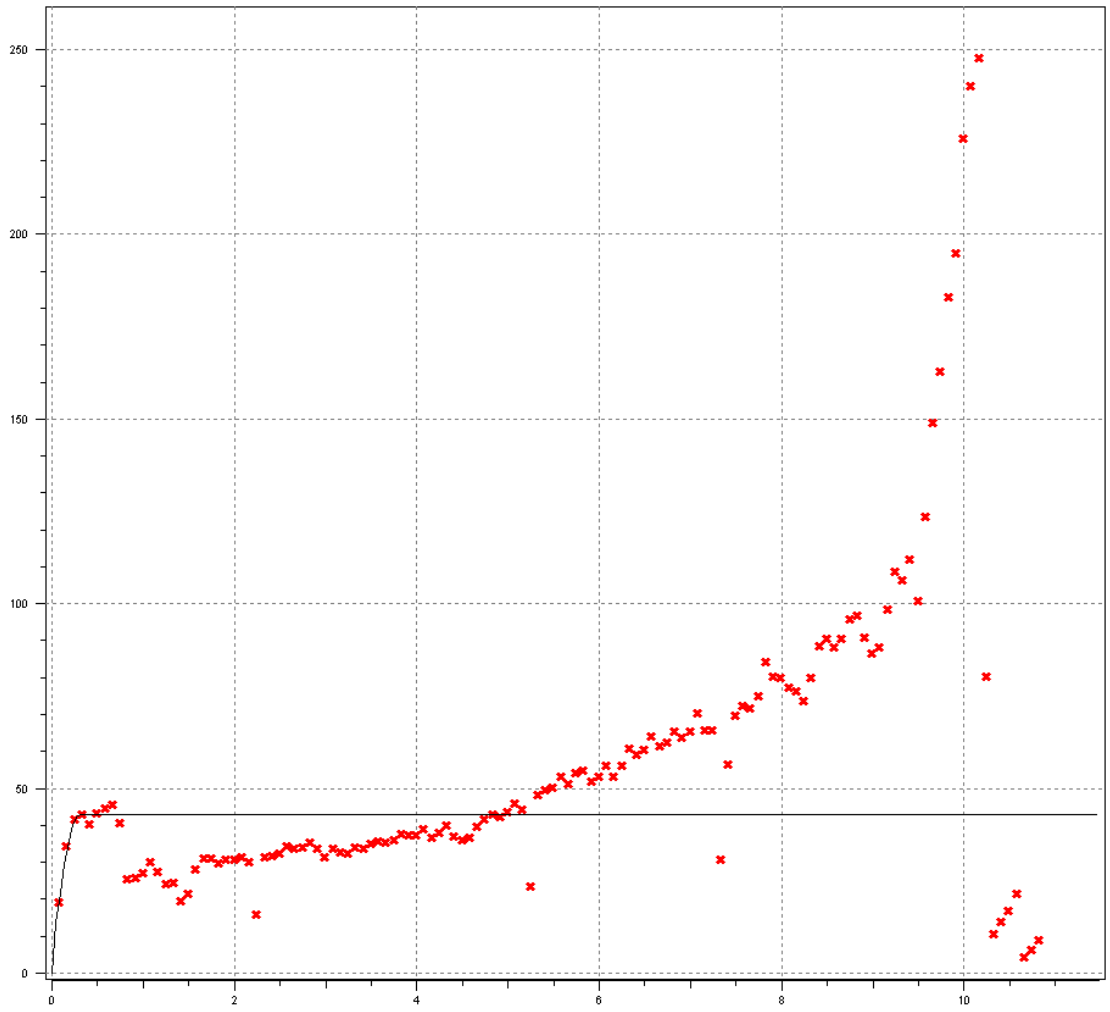

Fig. 3.2—Well 1 Towanda vertical variogram with spherical model.

The measured section of core is slightly over 10 feet long for the Well 1 Towanda member. Neglecting the hole-effect, a trend is evidenced by the increasing variance with distance. This variogram behavior is expected, since changing sea level produced a marine-continental cycle across productive members in the Hugoton Field (Dubois et al., 2006). The points on the variogram with the most supporting data are the points closest to zero on the abscissa. This is because there are more data pairs at a close

separation distance (e.g., a couple of inches) than there are data pairs with a farther separation distance (e.g., a couple of feet). Therefore, the model fitting will rely most strongly on these first few variogram points.

The measured section of core is slightly over 10 feet long for the Well 1 Upper Fort Riley member (**Fig. 3.3**).

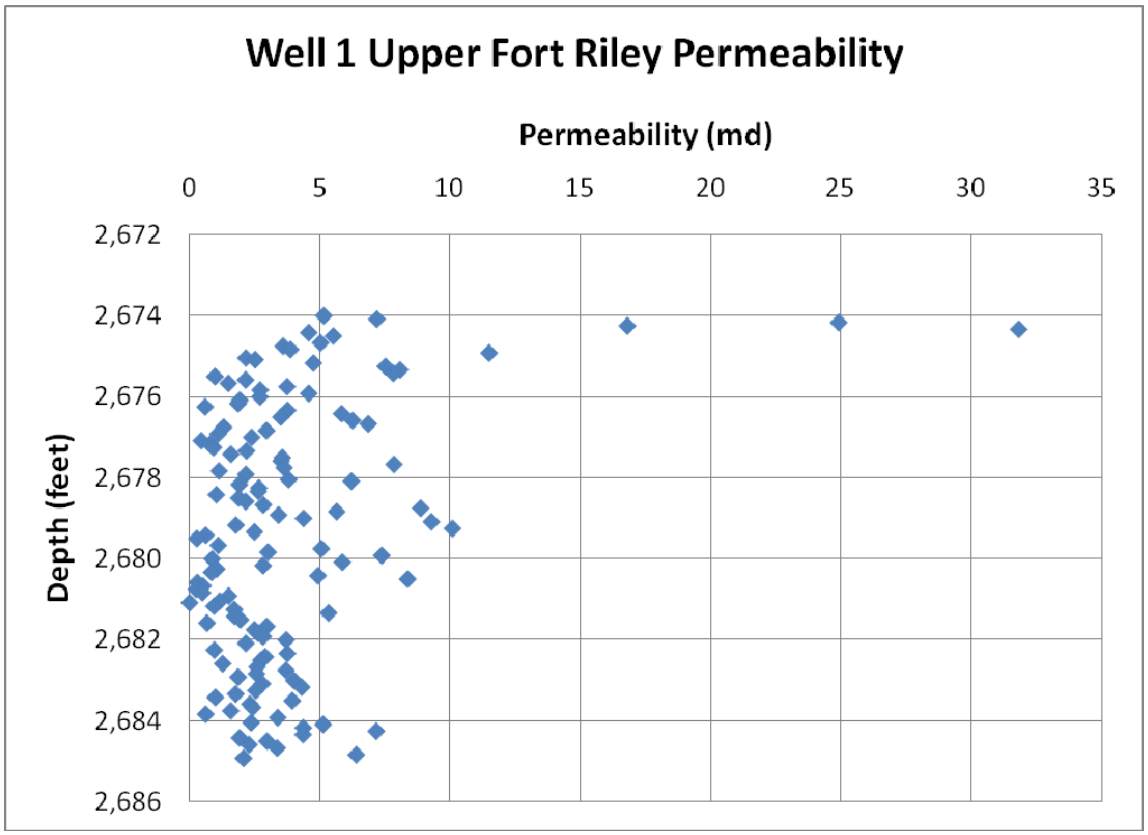

Fig. 3.3—Well 1 Upper Fort Riley slabbed core permeability.

Two scales of cyclicity are observed on the variogram for this member (**Fig. 3.4**).

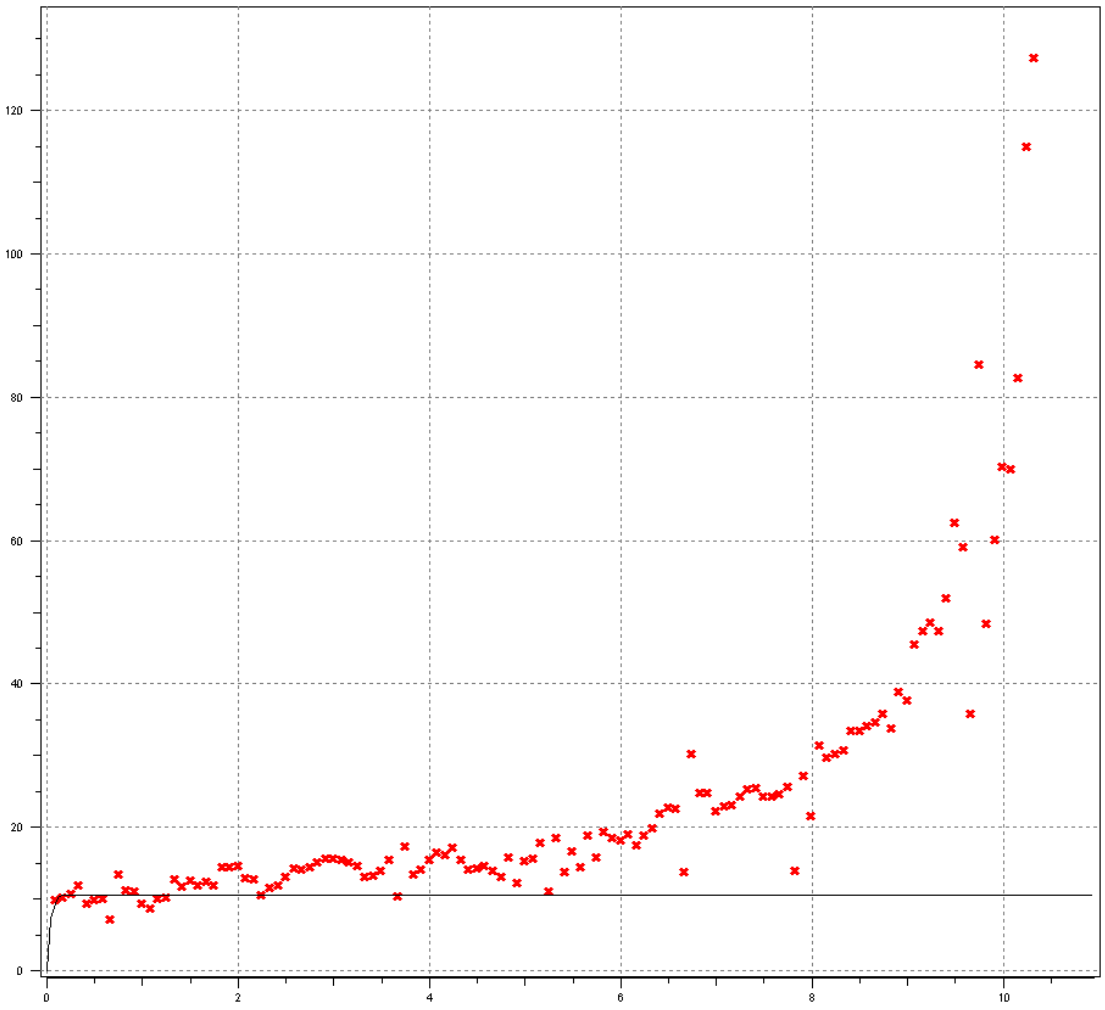

Fig. 3.4—Well 1 Upper Fort Riley vertical variogram with spherical model.

The small scale cycles repeat over a period of approximately 1 to 3 feet. The variogram model is fit to this trend. The larger cycle is a trend that occurs across the member due to sea level change (Dubois et al., 2006).

The measured section of core is slightly over 10 feet long for the Well 1 Lower Fort Riley member (**Fig. 3.5**).

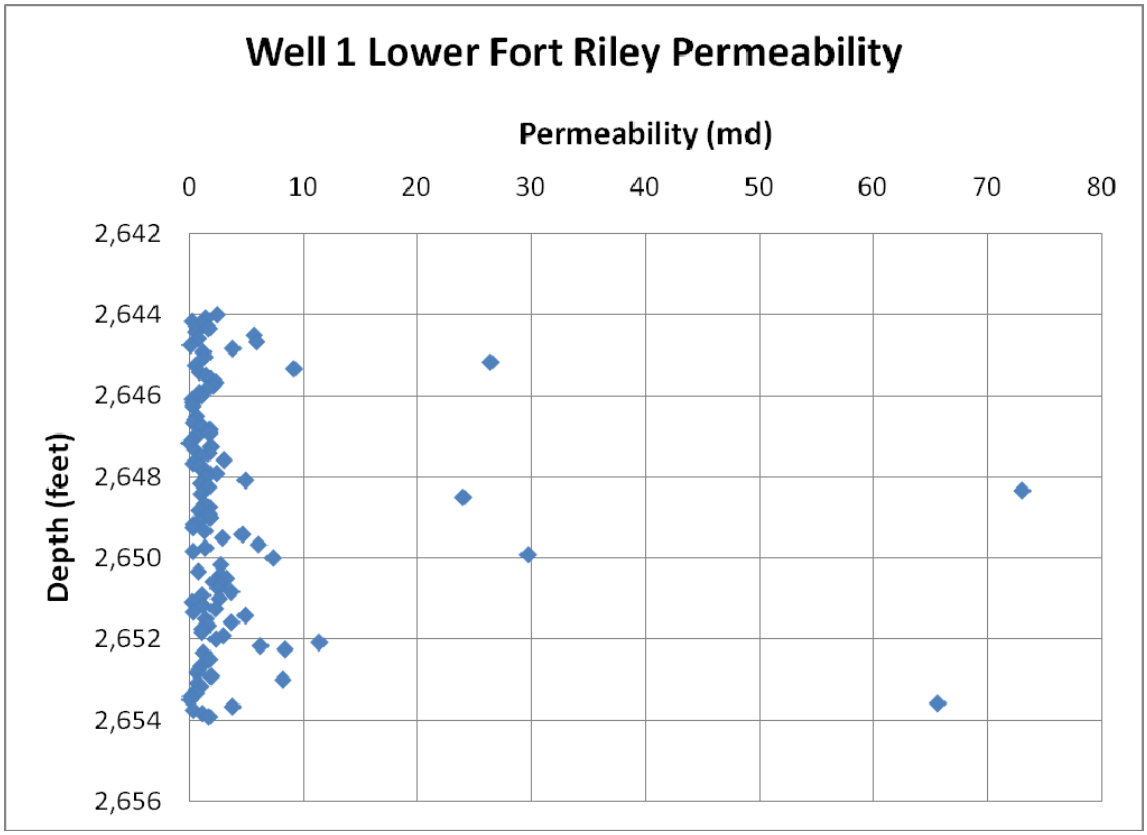

Fig. 3.5—Well 1 Lower Fort Riley slabbed core permeability.

This member has a small scale cyclicity that is observable on both the graph of permeability and the variogram (**Fig. 3.6**).

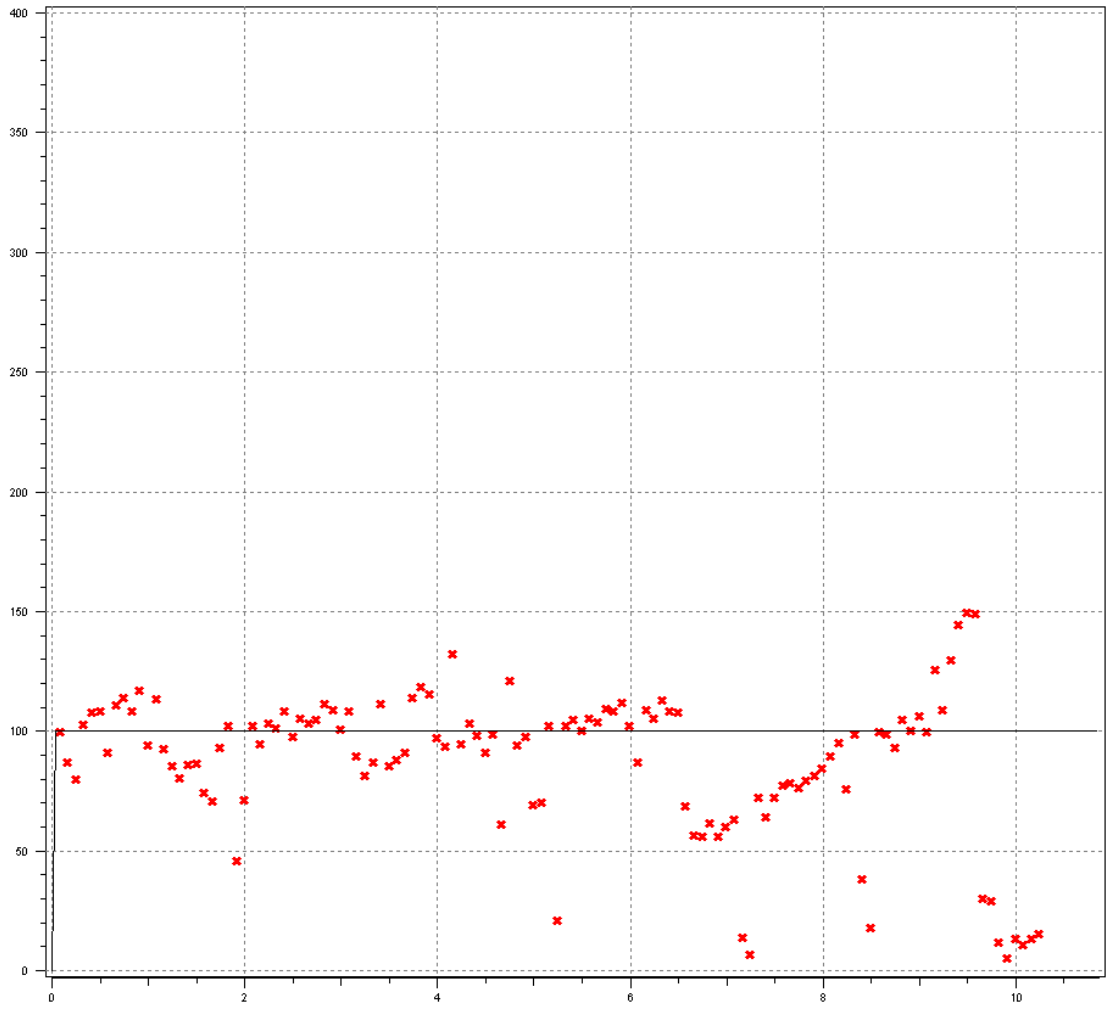

Fig. 3.6—Well 1 Lower Fort Riley vertical variogram with pure nugget model.

The small scale cycles repeat over a period of roughly 4 to 6 feet. Surprisingly, the variogram for this member does not show a larger cyclicity or trend even though a symmetric sea level change is typical of the Fort Riley member (Dubois et al., 2006). Despite the small scale cyclicity, the scatter in permeability data is sufficient to result in a very low correlation length, which is below the measurement separation distance of

one inch. Therefore, a pure nugget variogram model is used and the vertical correlation length is essentially zero for this member.

Segments of high permeability (k_{air} > 10 md) occur at two locations along the Well 2 Towanda member 10 foot segment of measured core (**Fig. 3.7**).

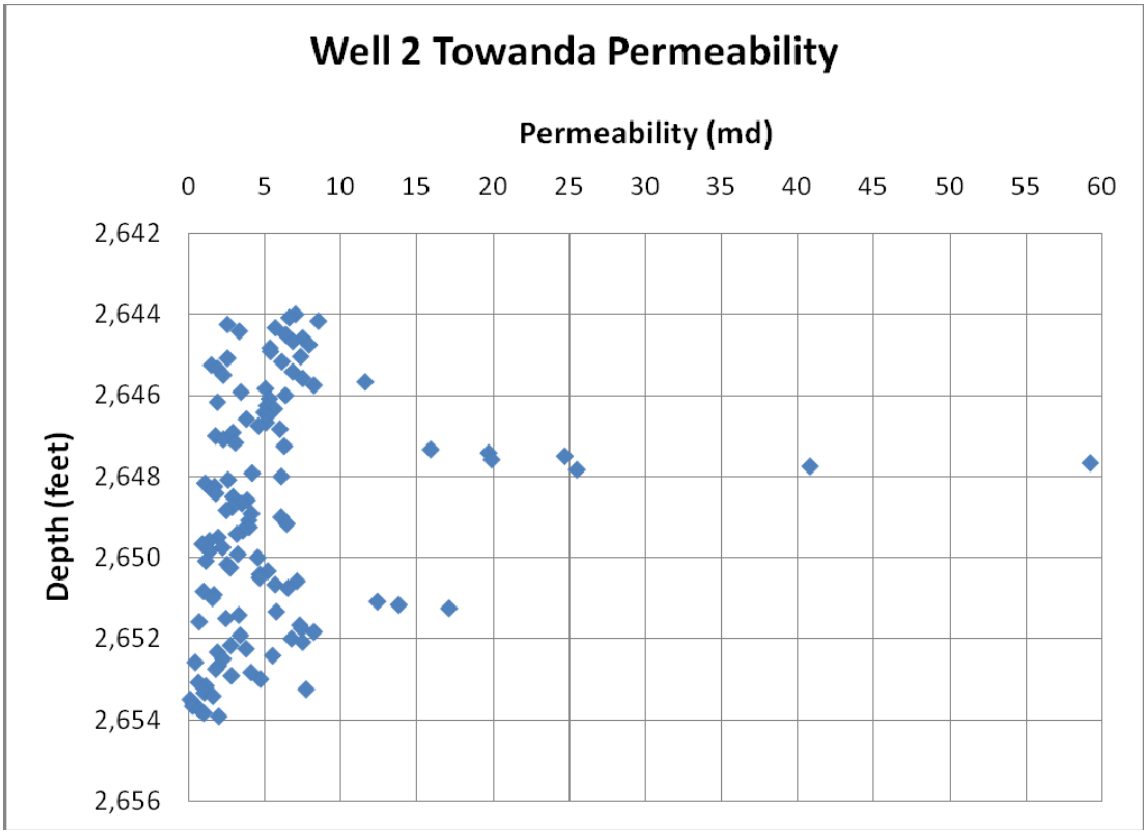

Fig. 3.7—Well 2 Towanda slabbed core permeability.

These segments of higher permeability cause a cyclical structure to be readily apparent on the variogram (**Fig. 3.8**).

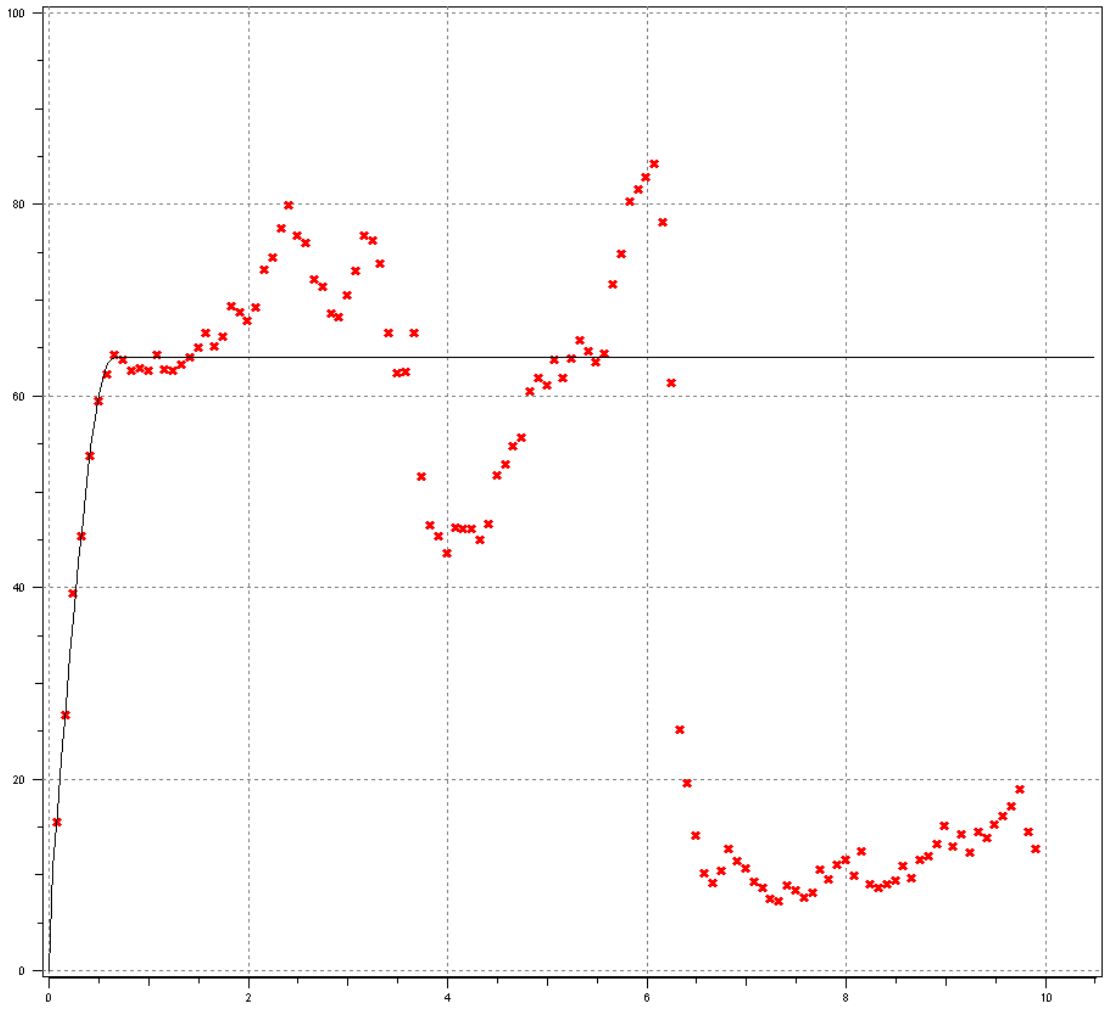

Fig. 3.8—Well 2 Towanda vertical variogram with spherical model.

The segments of core with higher permeability represent the two peaks observed in this variogram, creating an obvious hole-effect between the observed peaks. The higher streaks of permeability limit the vertical correlation, but the lower variance observed past a separation distance of 6 feet implies a larger scale of cyclicity across this member. Scales of permeability correlation exist across the Towanda member, indicating that the separation distance selection for permeability measurements is a critical

experimental design criterion affecting significantly the estimated correlation length. Denser data results in finer resolution of cycles that may contribute to acid fracture conductivity.

Each cycle has the potential to contribute to the overall etching pattern, since fractures may extend hundreds of feet in height and length. However, the Mou et al. (2010) correlations only allow one overall correlation length to be input for the calculation of conductivity, and the model was developed based on 10 foot by 10 foot grid blocks. The correlation length most appropriate for use in the correlations is the one supported across the 10 foot by 10 foot grid block domain. The correlation length most strongly supported by the permeability data is the first one observed starting at zero on the abscissa, since these variogram data points have the highest number of compared data pairs included in their calculation. Therefore, the first correlation length observed on each variogram is the one that will be used in the conductivity correlations.

A segment with higher permeability is also apparent toward the center of the Well 2 Upper Fort Riley measured core section (**Fig. 3.9**).

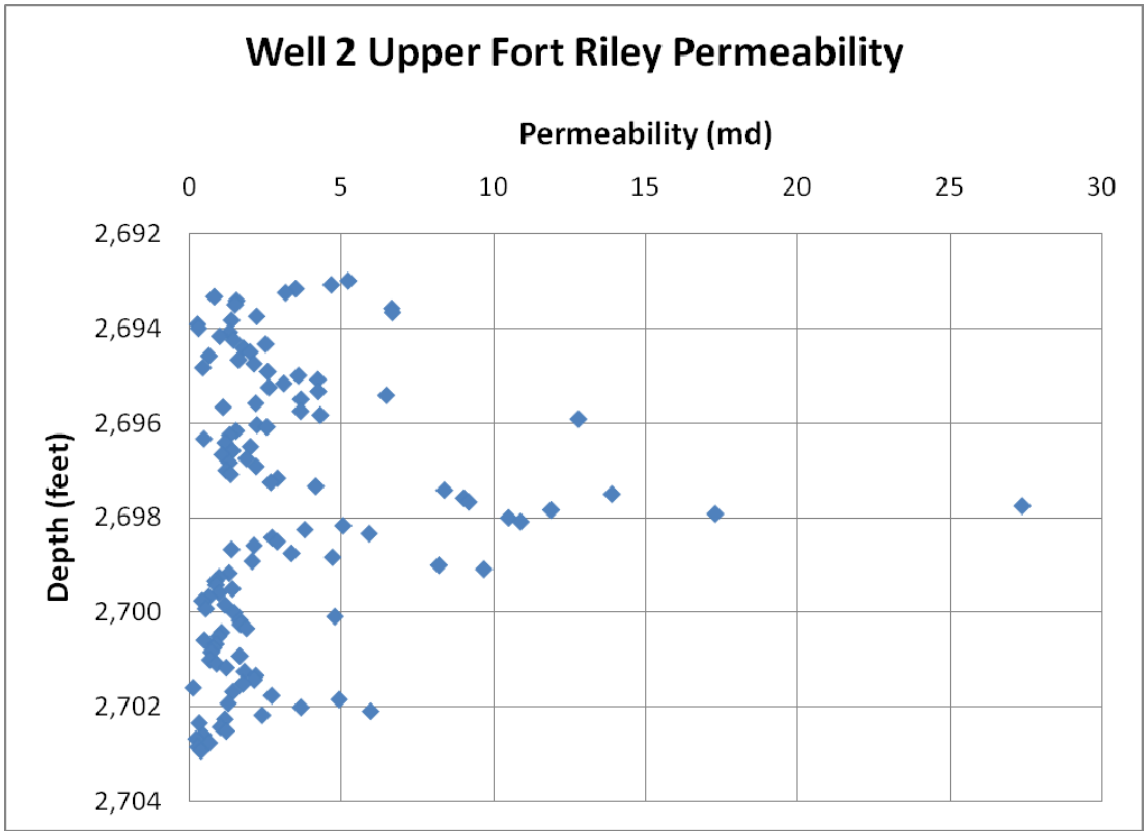

Fig. 3.9—Well 2 Upper Fort Riley slabbed core permeability.

These higher permeability measurements limit the correlation length observed on the member variogram (**Fig. 3.10**).

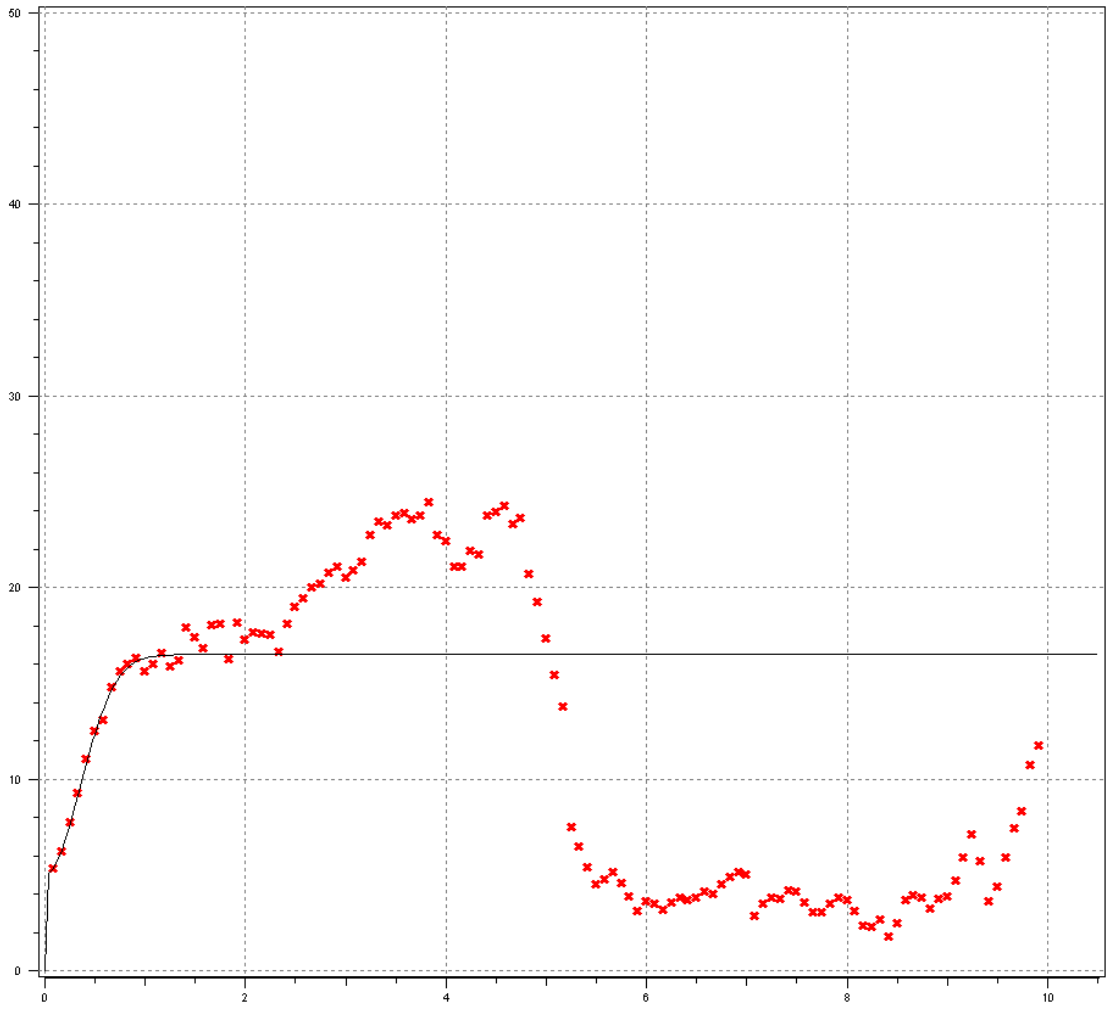

Fig. 3.10—Well 2 Upper Fort Riley vertical variogram with Gaussian model.

Some cyclicity is apparent, but the first structure is all that is relevant to the Mou et al. (2010) acid fracture conductivity correlations. The layer of high permeability causes a variance maximum with the lower variance observed past a separation distance of 5 feet, implying a larger scale of cyclicity across this member.

The Well 2 Lower Fort Riley measured portion of the member contained sandy regions with permeability over one Darcy. These measurements are not shown on the figure but range up to 1,066 md (**Fig. 3.11**).

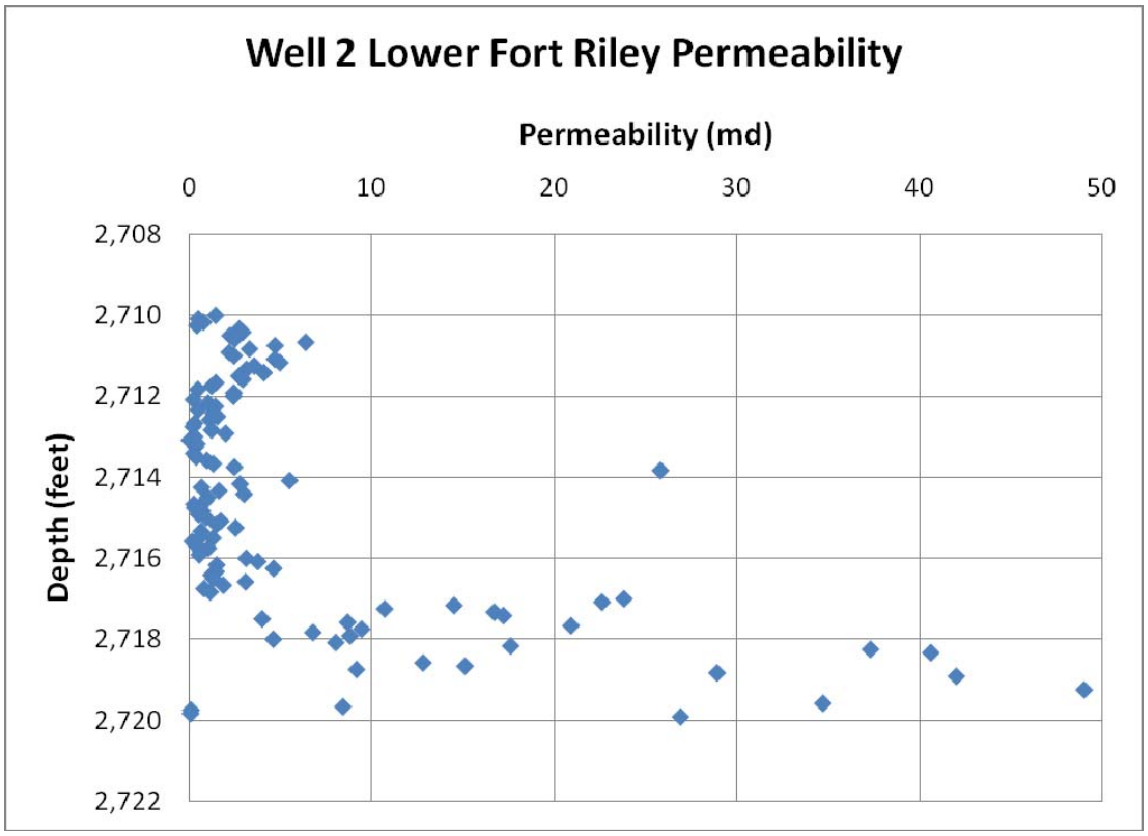

Fig. 3.11—Well 2 Lower Fort Riley slabbed core permeability.

Rock with this degree of dissimilarity is known to occur in portions of the Hugoton Field and represents a quickly changing depositional environment (Dubois et al., 2006). The trend toward more permeable rock is readily observed on the variogram for the Well 2 Lower Fort Riley member (**Fig. 3.12**).

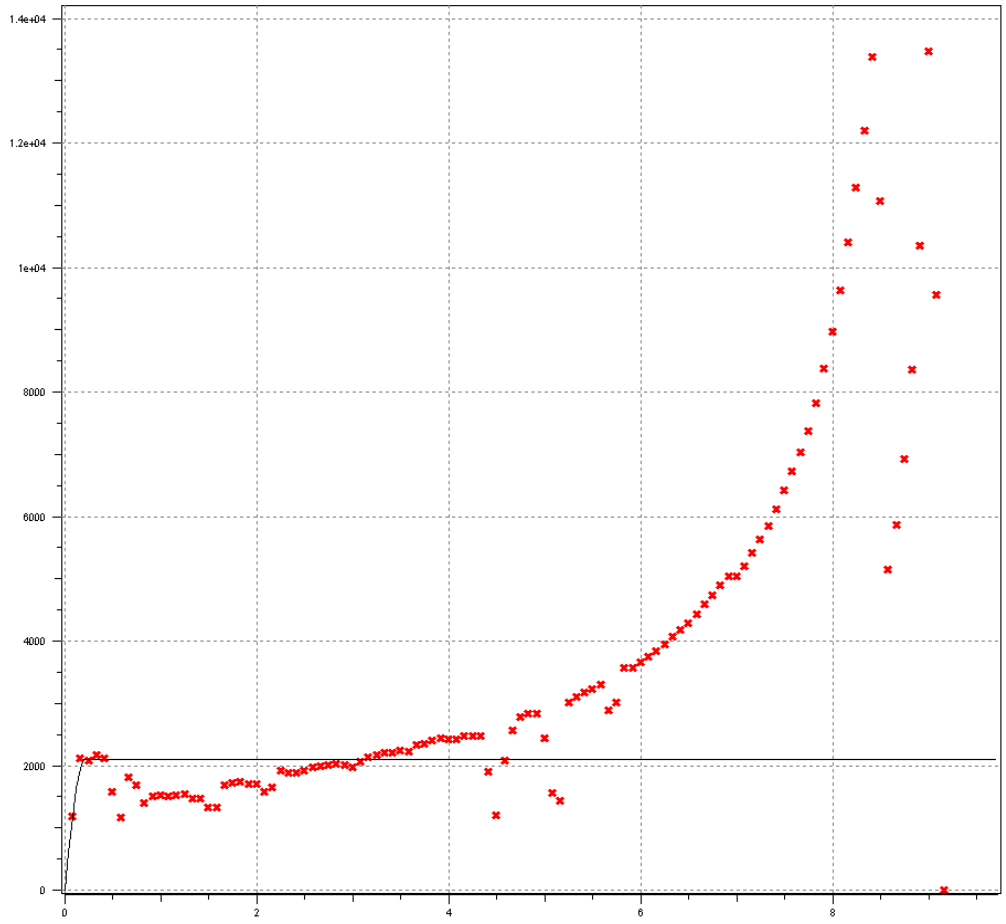

Fig. 3.12—Well 2 Lower Fort Riley vertical variogram with spherical model.

A hole-effect is also observed at a separation distance between 0.5 and 3.5 feet on the variogram. As with the Towanda member, varying scales of correlation are readily observed across the entire Fort Riley. The Mou et al. (2010) correlations will not capture this degree of complexity with respect to trends in formation properties.

Table 3.1 summarizes the vertical correlation lengths measured along each 10 foot section of slabbed core.

Table 3.1-Summary of vertical correlation lengths.

Well No.	Geologic Member	Vertical Correlation Length (ft)	Dimensionless Vertical Correlation Length, $\lambda_{D,z}$
1	Towanda	0.300	0.0300
1	Upper Fort Riley	0.150	0.0150
1	Lower Fort Riley	< 0.083	≈ 0.0000
2	Towanda	0.645	0.0645
2	Upper Fort Riley	0.850	0.0850
2	Lower Fort Riley	0.202	0.0202

Based on the variogram models, the Lower Fort Riley member has the shortest vertical correlation length. The Towanda member in Well 1 has the highest correlation length for this well, but the Upper Fort Riley member has the highest correlation length for Well 2. This could be due to a difference in layering. Well 1 is observed to be significantly more layered than Well 2, which contains more homogeneous productive members. The higher degree of layering in Well 1 would also account for the lower overall correlation lengths. Even slight changes in depositional environment can cause significant petrophysical property variations.

The slabbed core was observed to be highly fractured. Drill stem test and core plug permeability data indicate that many wells in the Hugoton Field have matrix control of flow, meaning the field is probably not naturally fractured to a significant degree (Dubois et al., 2006). Previous studies have even thrown out whole core petrophysical data because of the contribution of induced fractures to measured permeability (Dubois et al., 2006). Extreme care was taken to avoid core sections exhibiting induced fractures.

Given the radius of investigation for the PPP-250 equipment, the error contributed by induced fractures is expected to be small (Jones, 1992).

Well 2 is the well for which the case study will be completed. Well 2 will be a horizontal well and completed with multiple transverse fractures. The transverse fractures along the horizontal wellbore are expected to extend across all Chase Group and some Council Grove Group productive members. The $\lambda_{D,z}$ parameters calculated for the Well 2 Fort Riley and Towanda members will be directly applied to those zones, but a weighted average of these values will be used for other productive zones across which the fractures will extend. This is a reasonable assumption as most of the acid fracture conductivity is expected to be generated near the wellbore in the Towanda member, which is where the well will be completed.

3.2 Horizontal Correlation Length

Operator supplied permeability estimates served as the basis for definition of the horizontal or lateral correlation length. Porosity log data were used to develop a transformation to permeability based on measured core plug permeability for the well being studied. The operator supplied permeability data are confidential and not presented as part of this research.

Permeability estimates are available every 6 inches along the horizontal well, which is over 1,000 feet long and runs through the Towanda member. A potential completion design includes four transverse fractures. The perforations and fracture initiation length are 10 feet at each fracture stage along the horizontal well. Therefore,

permeability data along each 10 foot stage were analyzed using variogram models, which also coincides with the Mou (2009) model grid block dimensions. All variograms were prepared using SGeMS (Remy et al., 2008). Every variogram is a plot of variance, $\gamma(h)$, on the ordinate with respect to separation distance between data pairs, h, on the abscissa.

A Stage 1 variogram, using permeability estimates along the 10 foot fracture initiation stage, is presented in **Fig. 3.13**.

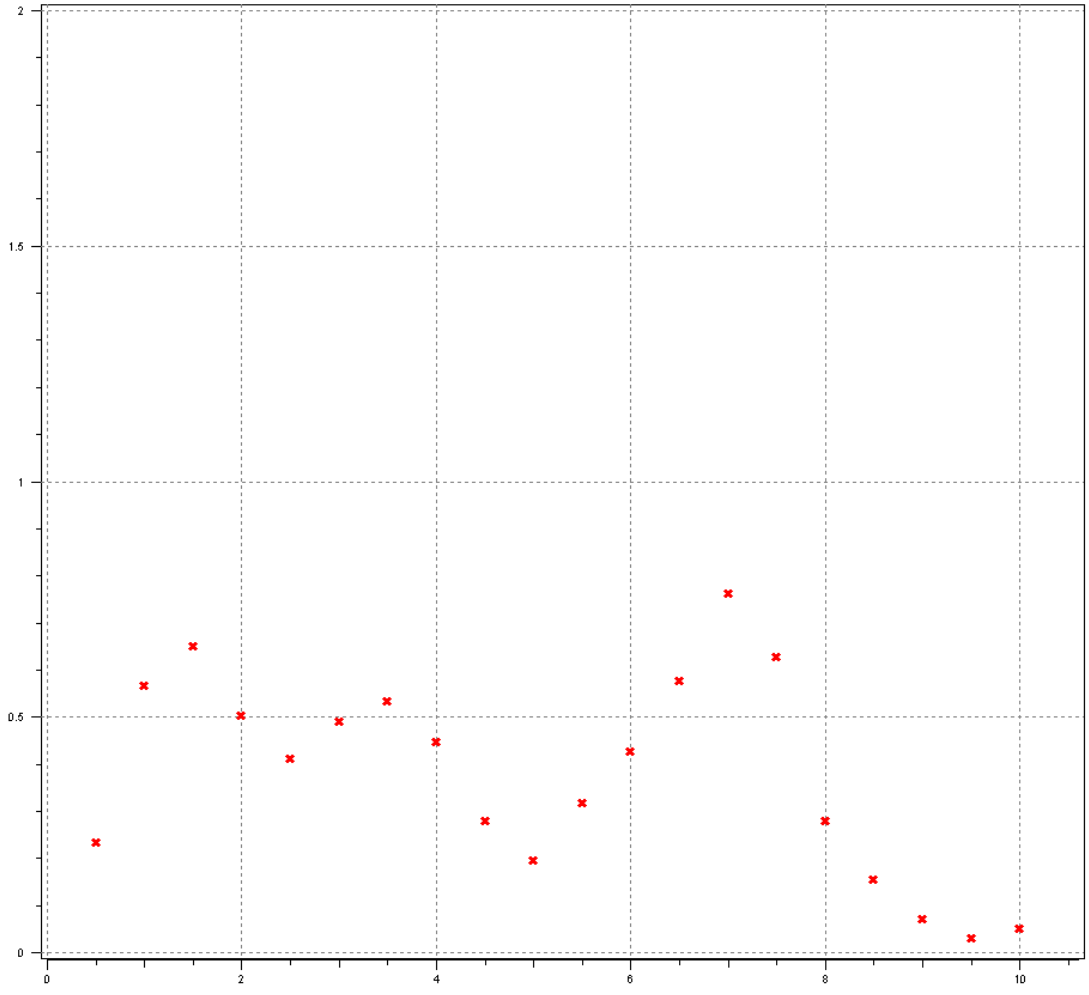

Fig. 3.13—Stage 1 variogram for 10 feet of permeability data.

The data points are separated by 6 inches, so a variogram using 10 feet of data results in only 20 data points. No structure is obvious using this amount of data. Therefore, a variogram using 30 feet of permeability data centered along the Stage 1 fracture initiation length was created (**Fig. 3.14**).

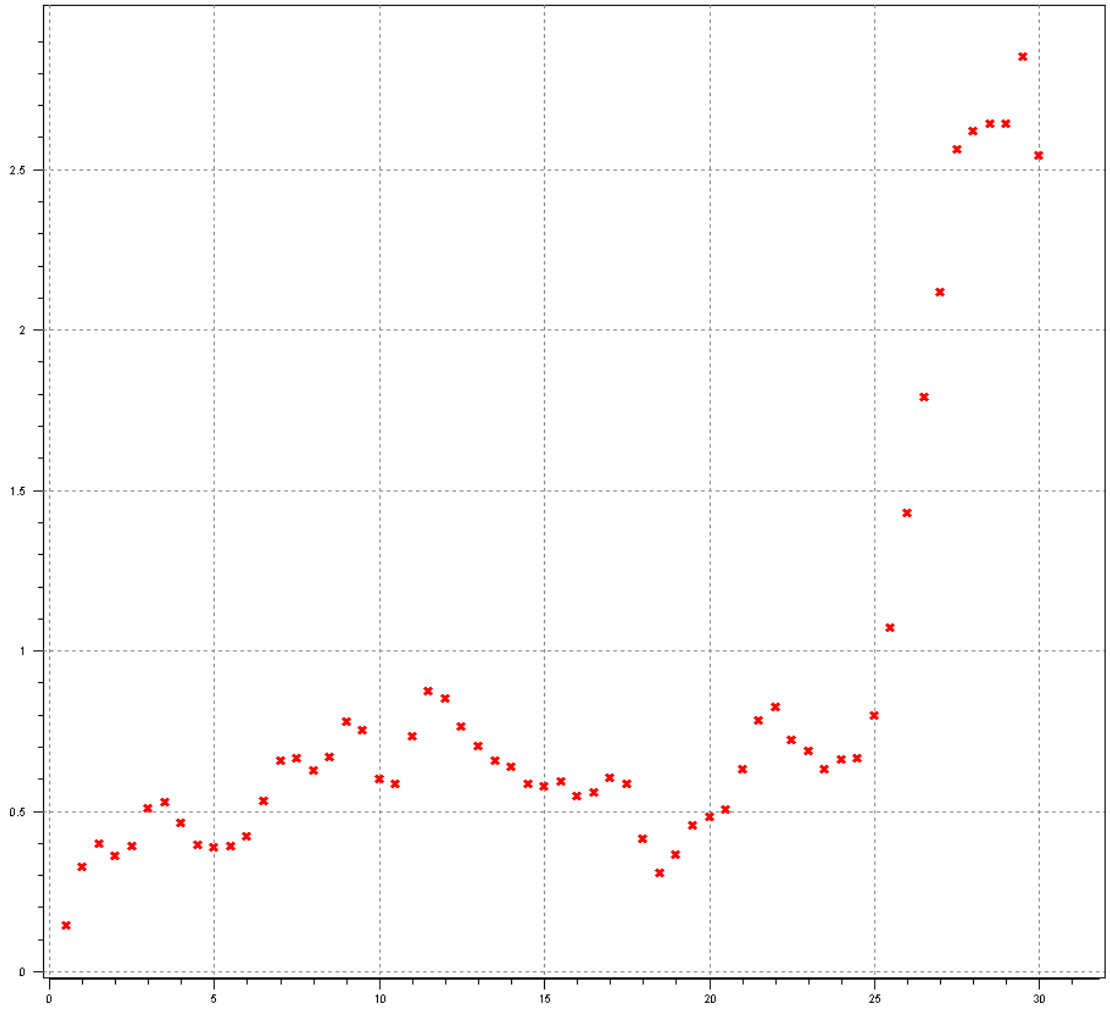

Fig. 3.14—Stage 1 variogram for 30 feet of permeability data.

The first geologic structure could have a correlation length of approximately 12 feet, but the variogram overall is still unclear using only 30 feet of permeability data. Therefore, a variogram using 50 feet of permeability data centered over the Stage 1 fracture initiation length was created (**Fig. 3.15**).

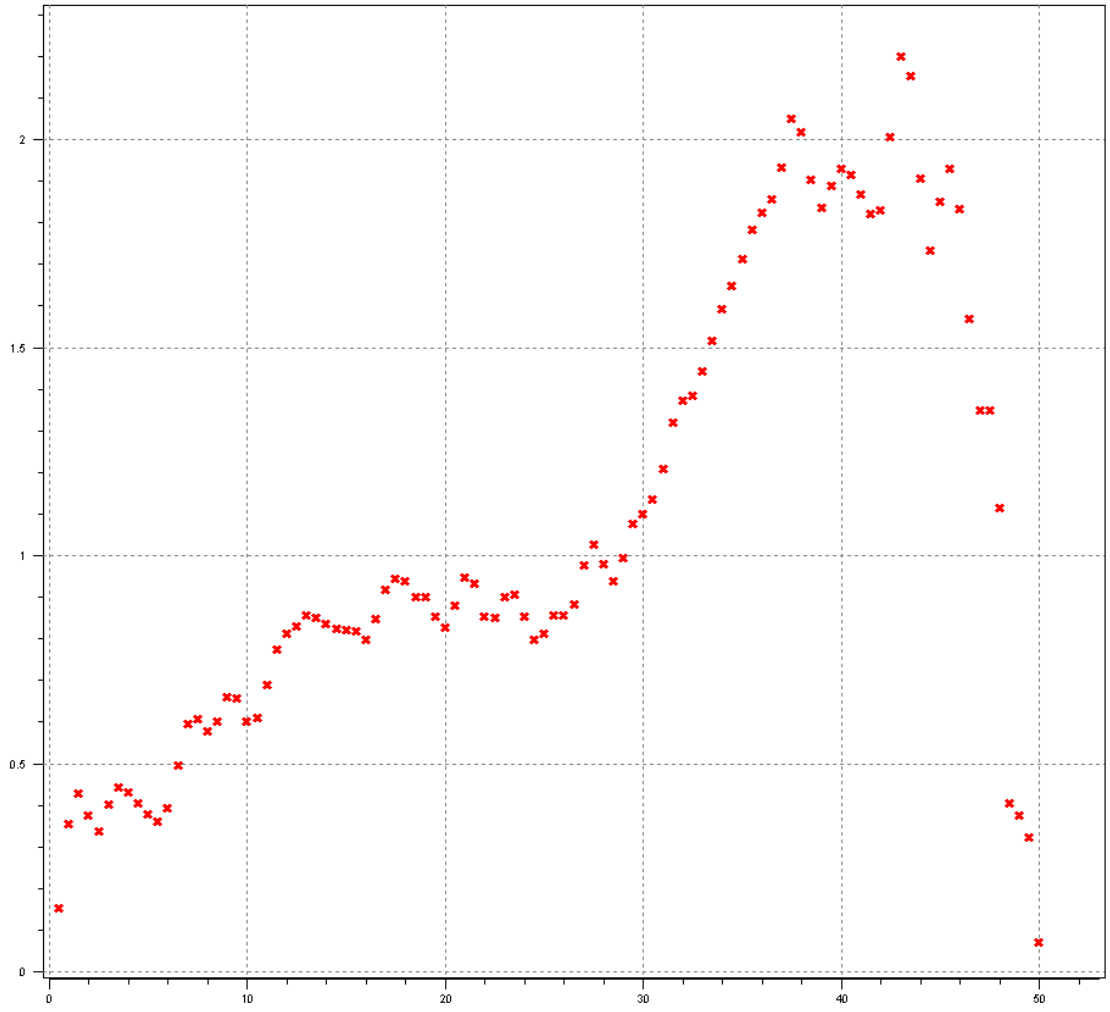

Fig. 3.15—Stage 1 variogram for 50 feet of permeability data.

The first geologic structure is beginning to appear despite interference from multiple scales of cyclicity. Tentatively, a correlation length near 20 feet appears, but an overall trend obscures the prevalence of this structure. Using 100 feet of permeability data, a variogram was created to resolve this uncertainty (**Fig. 3.16**).

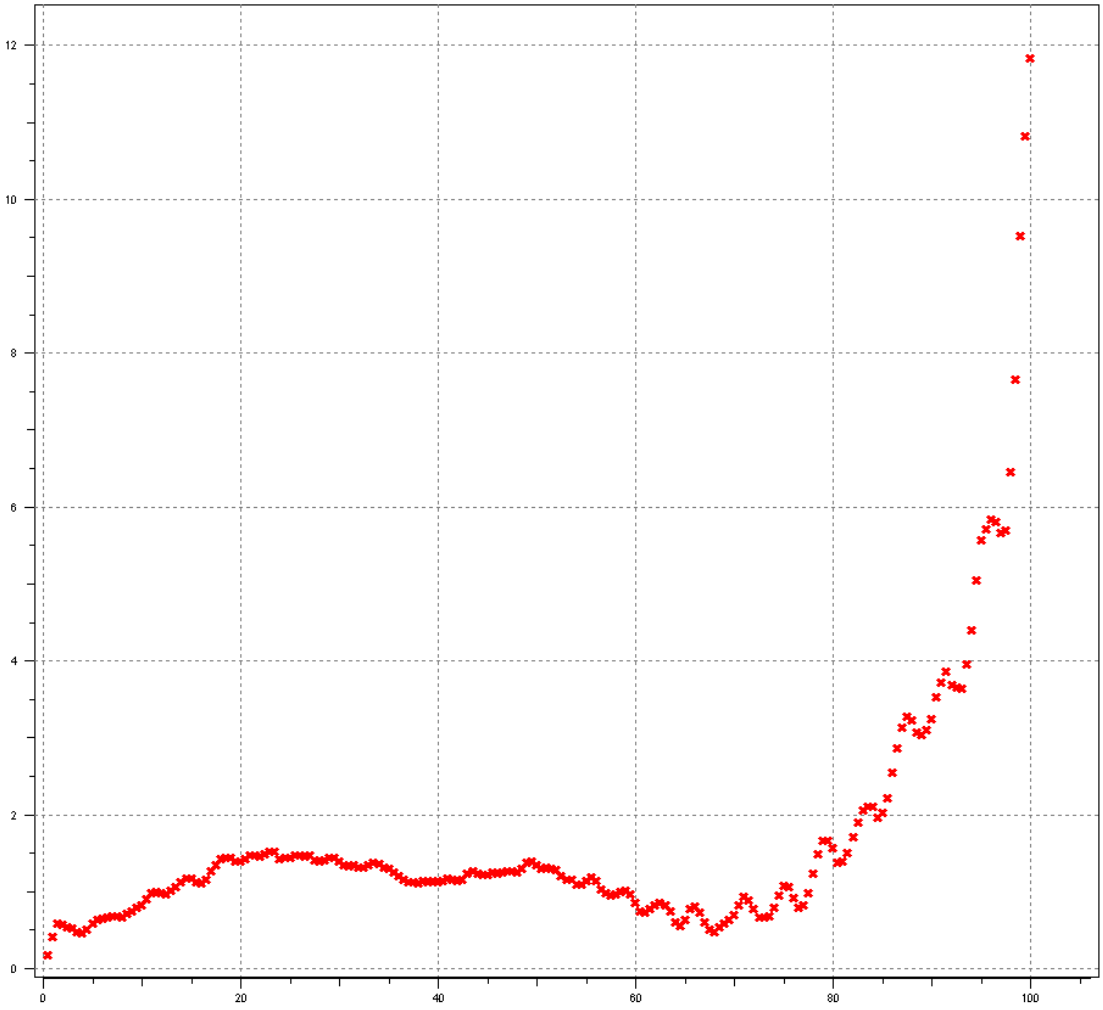

Fig. 3.16—Stage 1 variogram for 100 feet of permeability data.

The first geologic structure is now apparent. Confirming the appearance of this structure, variograms using 150 feet and 200 feet of data were created (**Figs. 3.17-3.18**).

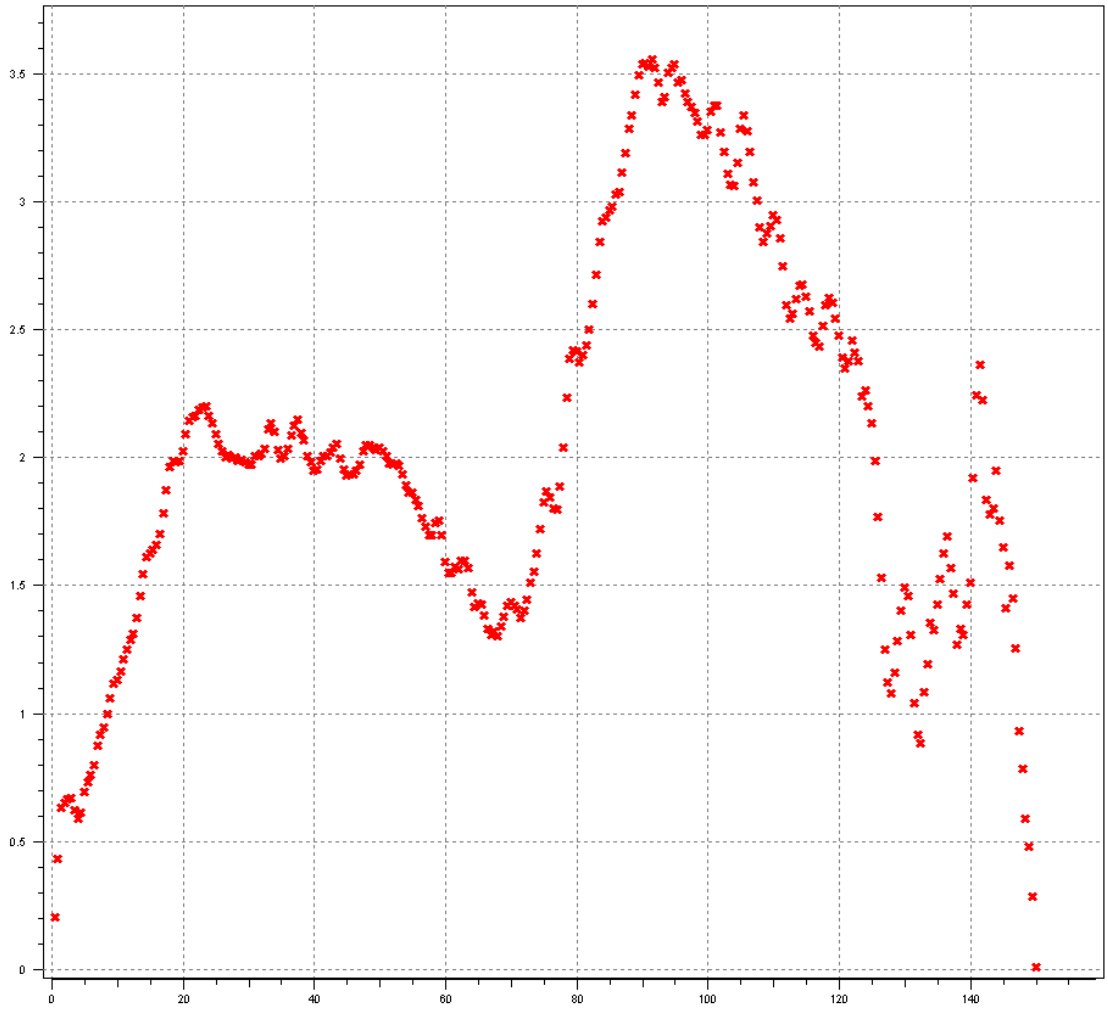

Fig. 3.17—Stage 1 variogram for 150 feet of permeability data.

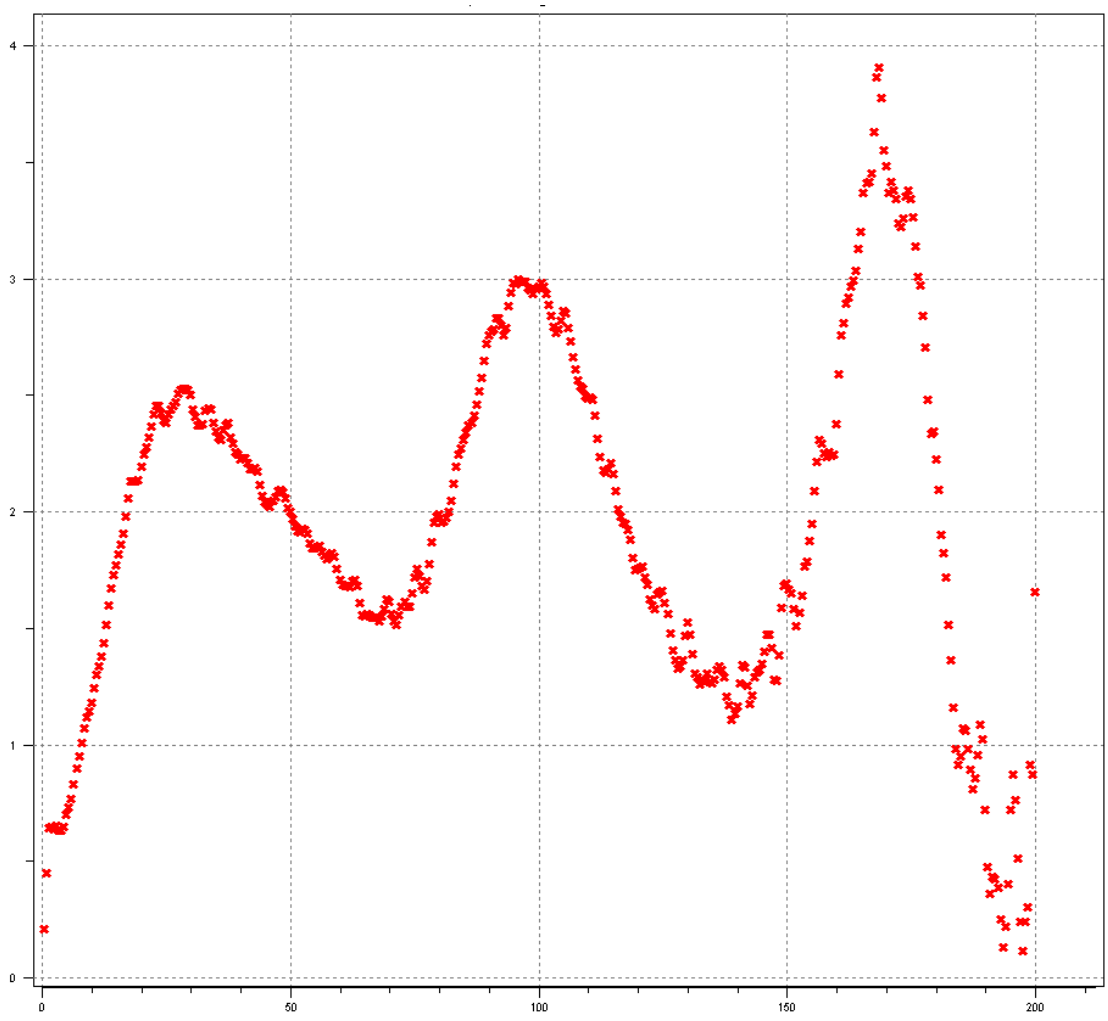

Fig. 3.18—Stage 1 variogram for 200 feet of permeability data.

Based on the variograms that use 150 and 200 feet of permeability data, the first structure correlation length is confirmed. To avoid missing small scale geologic structures, each variogram must be constructed from the smallest dataset possible. This limits the appearance of large scale structures that may occlude observation of the small scale heterogeneity relevant to acid fracture performance. Fitting a variogram model to the variogram that uses 200 feet of data, a correlation length is defined for the first

geologic structure observed along Stage 1. This procedure was used for Stage 2, Stage 3, and Stage 4 permeability data. The variograms created using only 10 feet of permeability data along each stage are presented (**Figs. 3.19-3.21**).

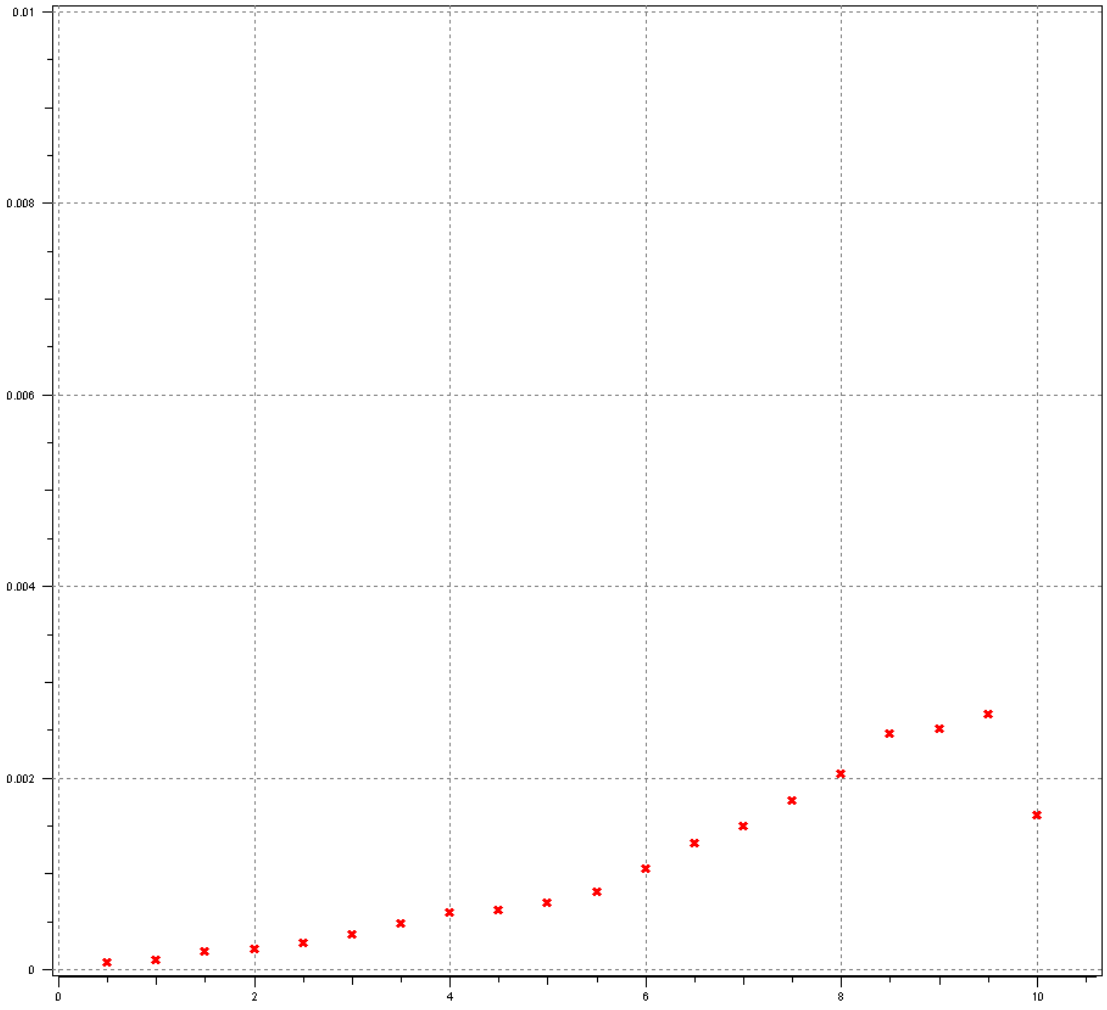

Fig. 3.19—Stage 2 variogram for 10 feet of permeability data.

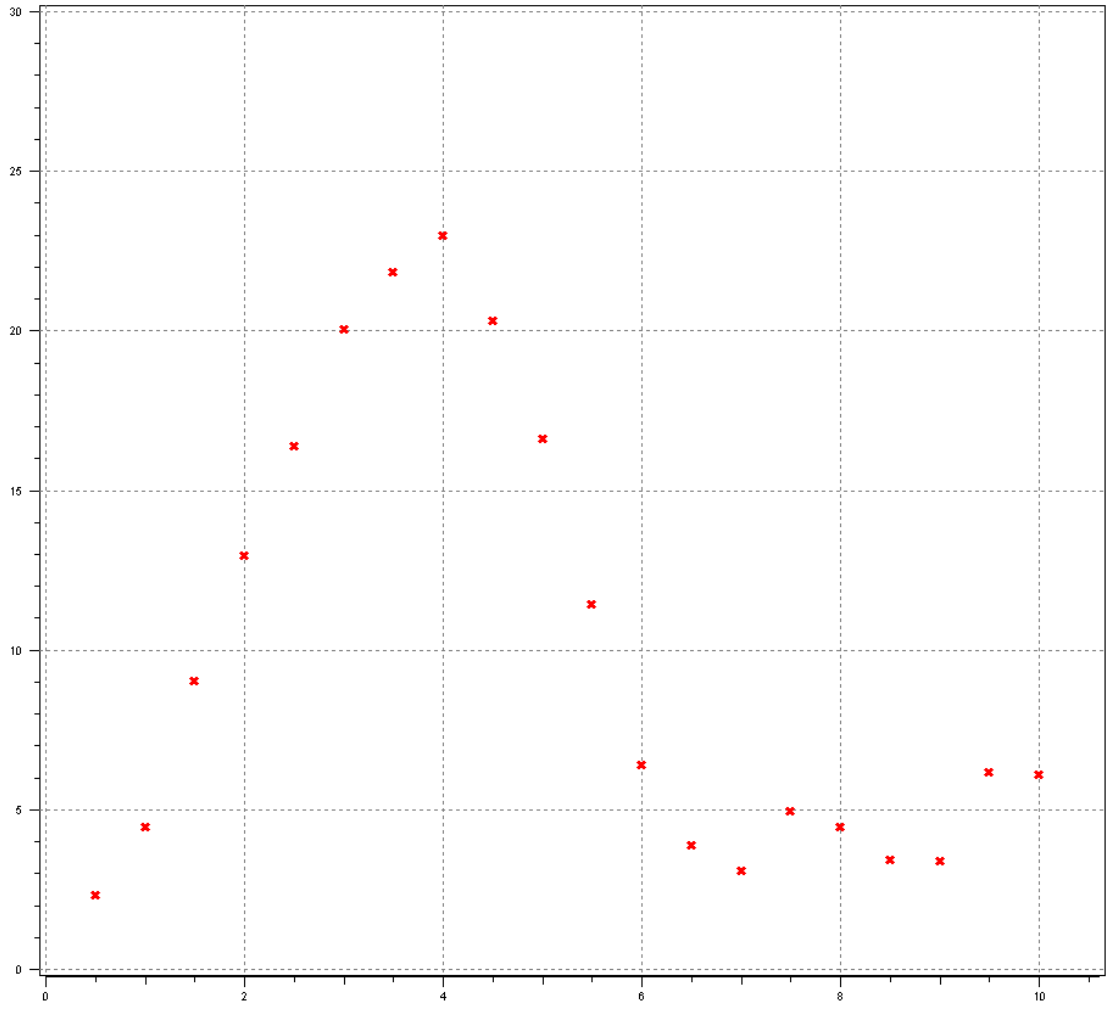

Fig. 3.20—Stage 3 variogram for 10 feet of permeability data.

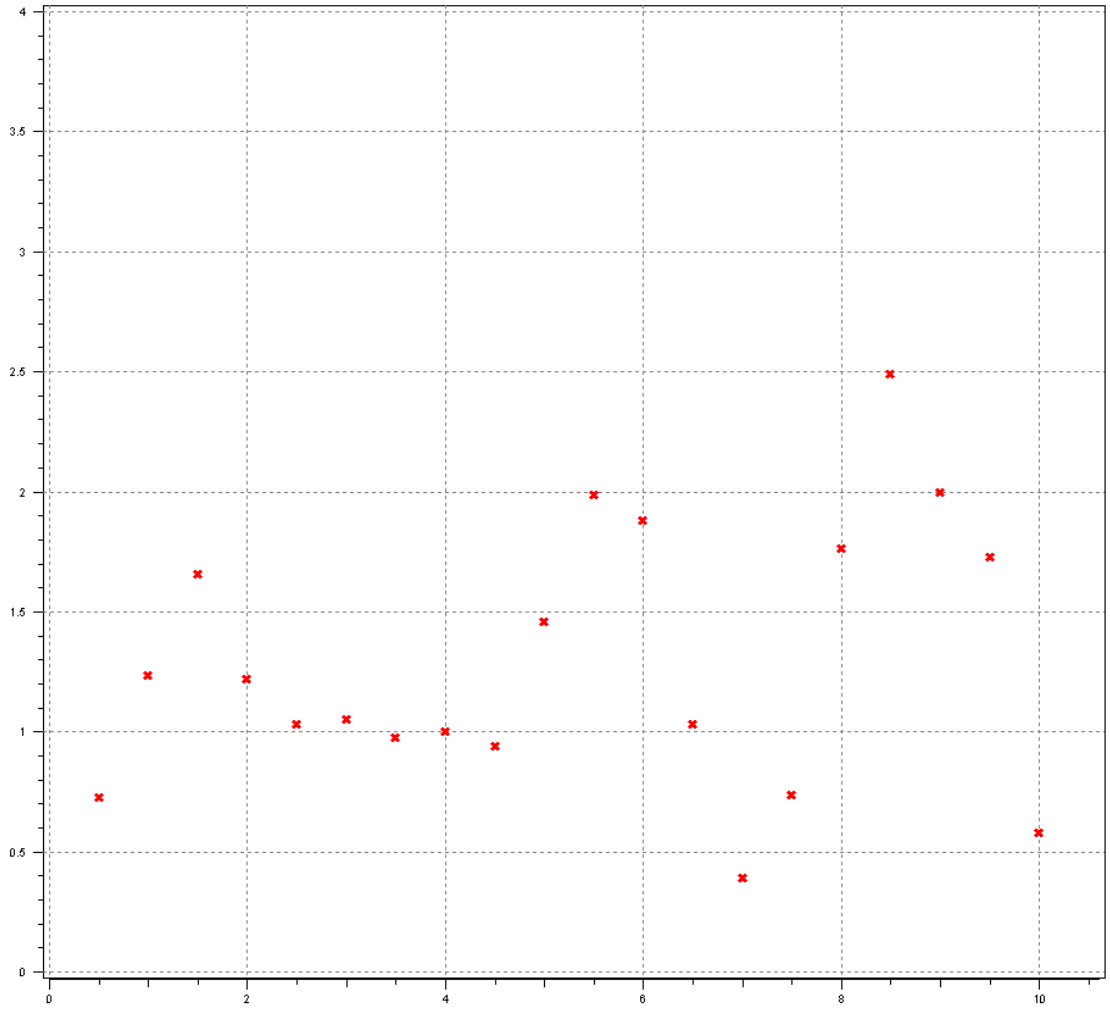

Fig. 3.21—Stage 4 variogram for 10 feet of permeability data.

Stage 2 displayed a long trend that was only resolved using 250 feet of permeability data for construction of the horizontal variogram (**Fig. 3.22**).

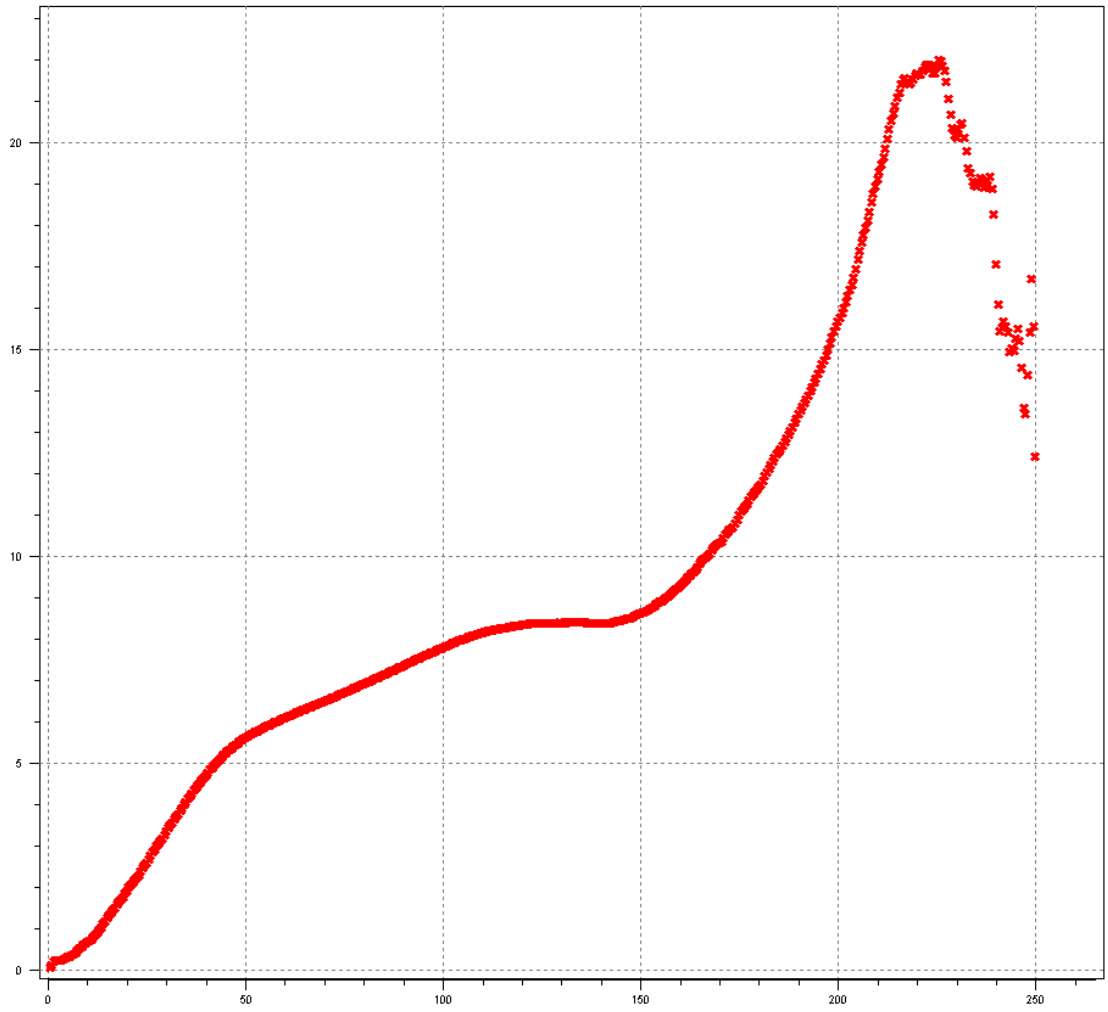

Fig. 3.22—Stage 2 variogram using 250 feet of permeability data.

The final variogram for Stage 2 reveals two competing structures, which have correlation lengths of 60 feet and 127.5 feet. Structures in Stage 3 were resolved when a variogram using 50 feet of permeability data was constructed (**Fig. 3.23**).

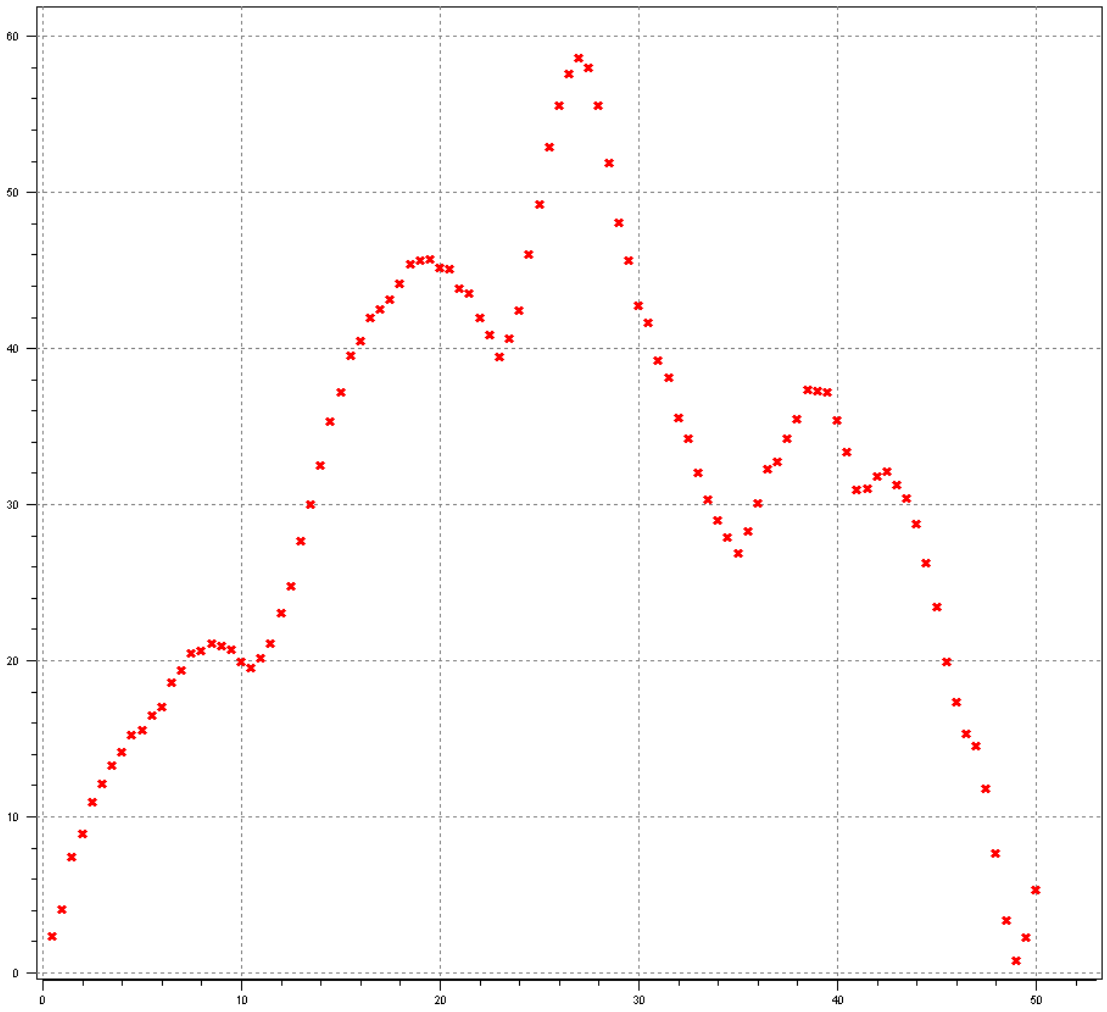

Fig. 3.23—Stage 3 variogram using 50 feet of permeability data.

The correlation length of the first geologic structure is 8.85 feet. This structure is not visible when larger sections of data are used to construct the variogram. Using 100 feet of permeability data to construct the Stage 3 variogram results in only one visible structure with a correlation length over 40 feet.

The Stage 4 variogram is constructed using 200 feet of permeability data to resolve a long lateral trend and determine a horizontal correlation length of 130 feet (**Fig. 3.24**).

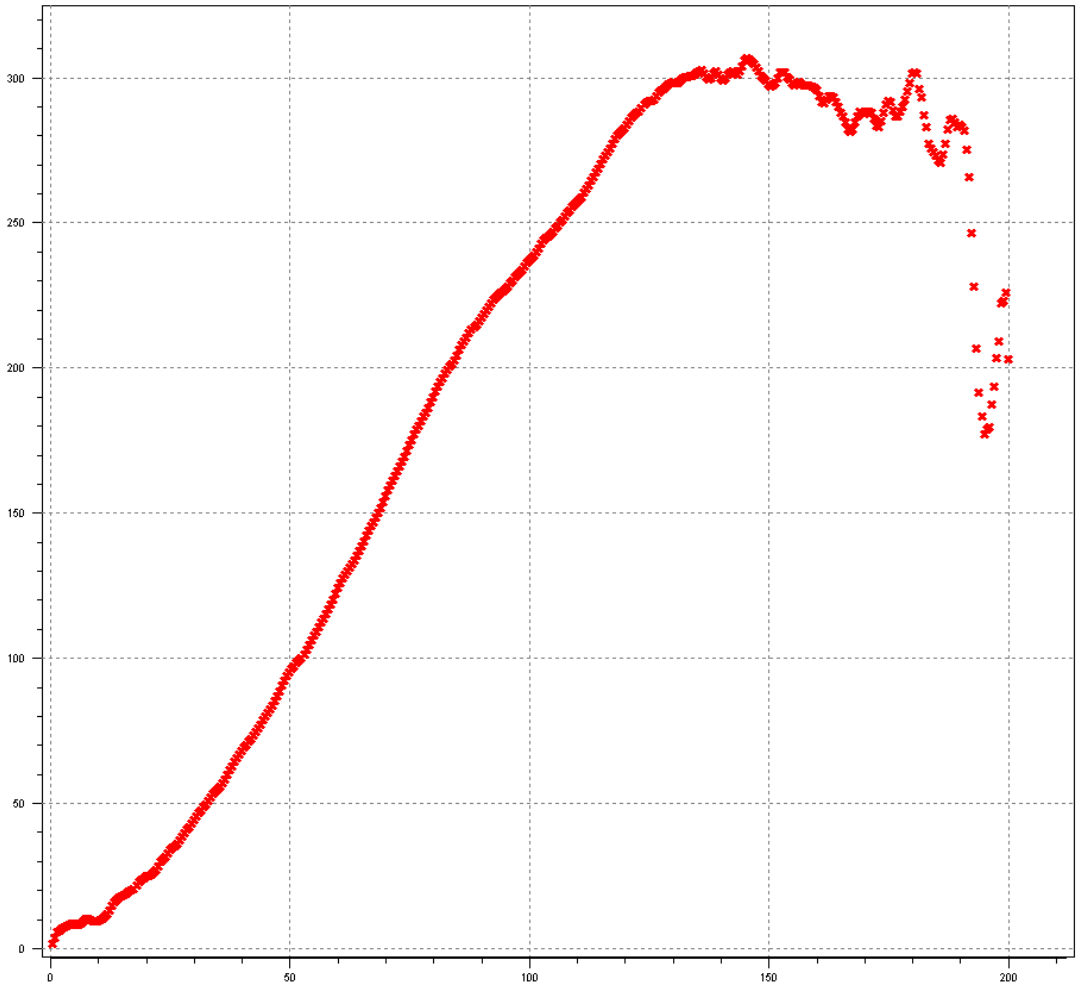

Fig. 3.24—Stage 4 variogram using 200 feet of permeability data.

Table 3.2 summarizes the horizontal correlation lengths estimated for each fracture stage.

Table 3.2-Summary of horizontal correlation lengths.

Stage	Horizontal Correlation Length (ft)	Dimensionless Horizontal Correlation Length, $\lambda_{D,x}$
1	26.25	1
2	60.0	1
3	8.85	0.885
4	130	1

The variogram models predict horizontal correlation based on k_H data. In reality, the acid fracture performance prediction requires k_{90} data for transverse fractures. However, given the extent of the Hugoton Embayment and associated marine shelf, it will be assumed that k_{90} is approximately equal to k_H. This may be a reasonable assumption due to the scale of the lateral wellbore compared to the ancient shelf environment.

The permeability estimates are made for the Towanda member as this is where the lateral has been drilled and will be completed, but the transverse fractures are expected to extend across all productive Chase Group members. The lack of available horizontal permeability data force the assumption that the horizontal geostatistical parameters developed for each stage along the Towanda will apply to the other members across which the transverse fractures extend. Sea level changes across each member are not necessarily symmetric (some changes occur more rapidly and to a greater degree than others). The extent of sea level change determines location on shelf and the series of depositional environments occurring across each productive member. Additionally,

the diagenetic history of the productive members is not the same. Therefore, the assumption that the horizontal geostatistical parameters are the same vertically along the transverse fracture at each stage is probably unreasonable. Due to the lack of data in the horizontal direction at a scale applicable to an acid fracture, however, this assumption is required for calculation of acid fracture conductivity using the Mou et al. (2010) correlations.

Where the correlation length exceeds the dimension of the Mou (2009) grid blocks, a dimensionless horizontal correlation length parameter of one is used. This results in the permeability at that grid block to be perfectly correlated in the x direction. In reality, the horizontal correlation length would result in an eventual termination of the permeability trend over the entire fracture domain. However, the Mou et al. (2010) conductivity correlations are applied discretely at each fracture grid block, so the effects of the larger trends observed in the horizontal permeability datasets are neglected.

3.3 Standard Deviation of Permeability

The dimensionless standard deviation of permeability, σ_D, must also be calculated to use the Mou et al. (2010) conductivity correlations. This requires calculating the standard deviation of the natural log of permeability , $\sigma(\ln(k))$, and the natural log of the average permeability, $\ln(\bar{k})$. This has been done using both the vertical and horizontal permeability datasets. Table 3.3 summarizes this data.

Table 3.3-Summary of the dimensionless standard deviation data.

Direction	Member or Stage	Dimensionless Standard Deviation, σ_D
Vertical	Well 1, Towanda	1.037
Vertical	Well 1, Upper Fort Riley	0.710
Vertical	Well 1, Lower Fort Riley	0.973
Vertical	Well 2, Towanda	0.552
Vertical	Well 2, Upper Fort Riley	0.866
Vertical	Well 2, Lower Fort Riley	0.586
Horizontal	1	0.137
Horizontal	2	≈ 1
Horizontal	3	0.047
Horizontal	4	0.164

The same permeability dataset that was used to construct the horizontal variograms was used to calculate the dimensionless standard deviation parameter with the exception of Stage 2. The permeability around Stage 2 exhibited three long trends ranging from just over 10 md to 0.001 md. This resulted in a very high dimensionless standard deviation parameter. The 250 foot dataset was broken into smaller sections and the σ_D term calculated over each smaller dataset. A more representative value of one was determined using smaller datasets (e.g., 50 feet centered around the fracture stage).

The average of the horizontal and vertical dimensionless standard deviation values will be used in the Mou et al. (2010) conductivity correlations for each stage. The σ_D parameters calculated for the Well 2 Fort Riley and Towanda members will be directly applied to those zones, but a weighted average of these values will be used for

other productive zones across which the fractures will extend. Except for Stage 2, the vertical σ_D are larger than the horizontal σ_D. This is expected given the larger correlation in the horizontal as opposed to the vertical.

4. CASE STUDY: ACID FRACTURE CONDUCTIVITY PREDICTION

4.1 Calculation of Ideal Etched Width

The detailed etching profile along the fracture is required to use the Mou et al. (2010) conductivity correlations. This requires the width, w_i, to be known as a function of position across the fracture. E-StimPlan 3D (Smith, 2008) is a fracture simulator developed by NSI Technologies that calculates acid etched width for a given acid fracture treatment. The major features of this program include:

- A fully implicit solution where fluid flow, fracture width, and fracture propagation/height growth are solved simultaneously
- 2D, multiphase solution for fluid flow (includes diffusion)
- Finite element method solution for calculation of fracture width and fracture propagation for formations with modulus variation across geologic layers
- Complete simulation of flowback after a treatment as the simulation will continue until the calculated bottomhole pressure at the fracture entrance is less than the hydrostatic head of water to the surface
- Calculation of Nierode-Kruk conductivity across the simulated fracture

The operator supplied all treatment parameters, including the detailed geologic layering specific to the well under study, modulus data, leakoff coefficients, detailed well completion, reservoir conditions, acid reaction rate parameters, fracture fluid properties, and pump schedule. The final calculated acid etched width for the fracture at each stage

is the same since all treatment, geologic, and reservoir parameters are assumed to be the same (**Fig. 4.1**).

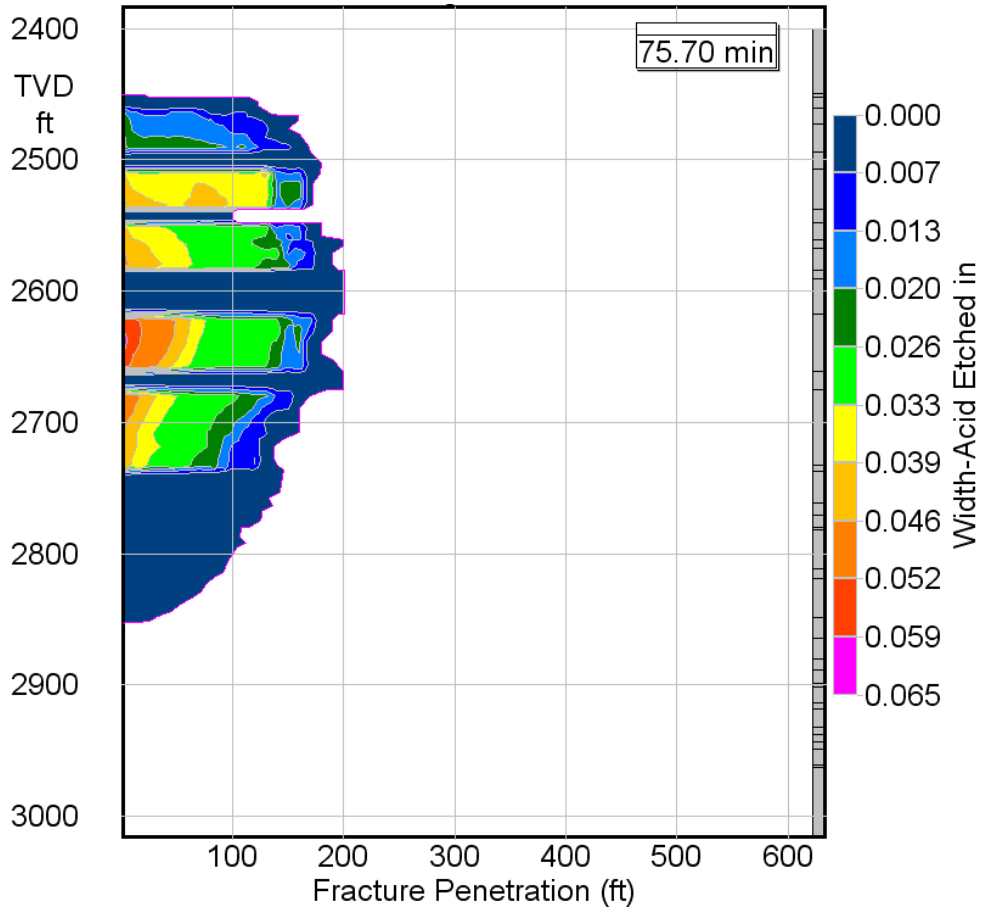

Fig. 4.1—Acid etched width across fracture.

4.2 Calculation of Conductivity

The E-StimPlan 3D (Smith, 2008) calculated Nierode-Kruk conductivity is the same for each stage since the acid etched width, rock embedment strength, and final closure stress (965 psi) are the same across each stage (**Fig. 4.2**).

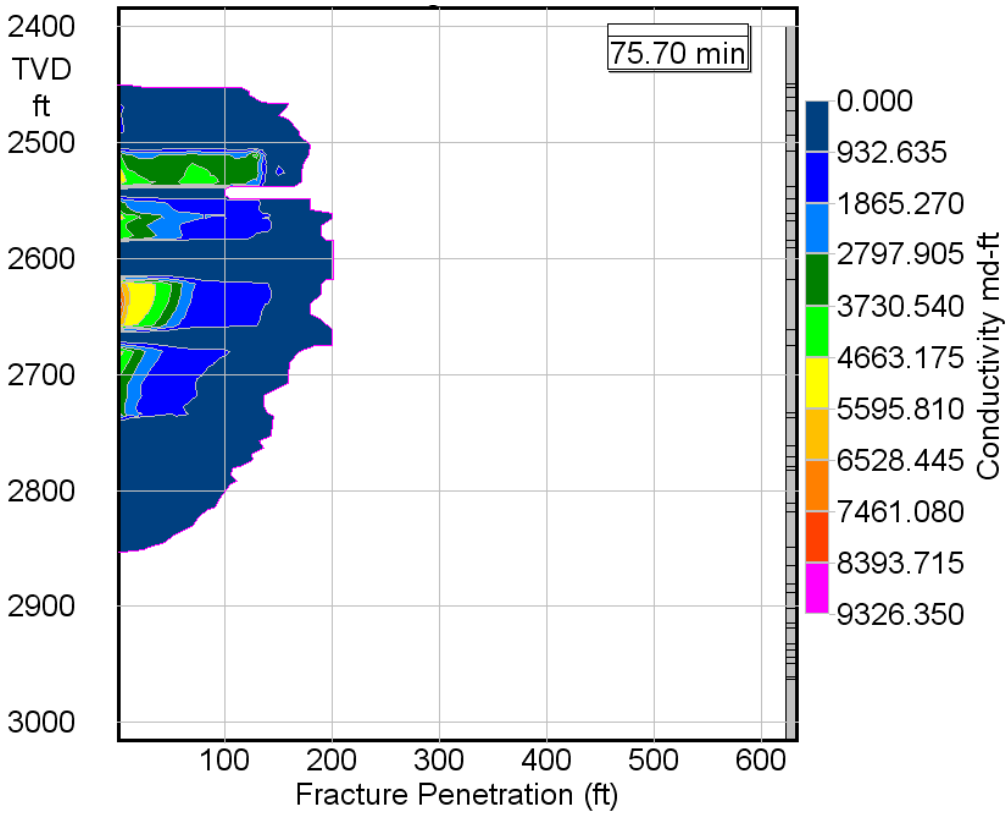

Fig. 4.2—Simulated Nierode-Kruk conductivity across fracture.

Only the top five producing members (Herington, Krider, Winfield, Towanda, and Fort Riley) are assumed to be able to generate substantial acid fracture conductivity even though other members contain carbonate material. For comparison to the Mou (2009) model, the Nierode-Kruk conductivity at zero closure stress is also computed based on the simulated closure stress (965 psi) and output conductivity (**Fig. 4.3**).

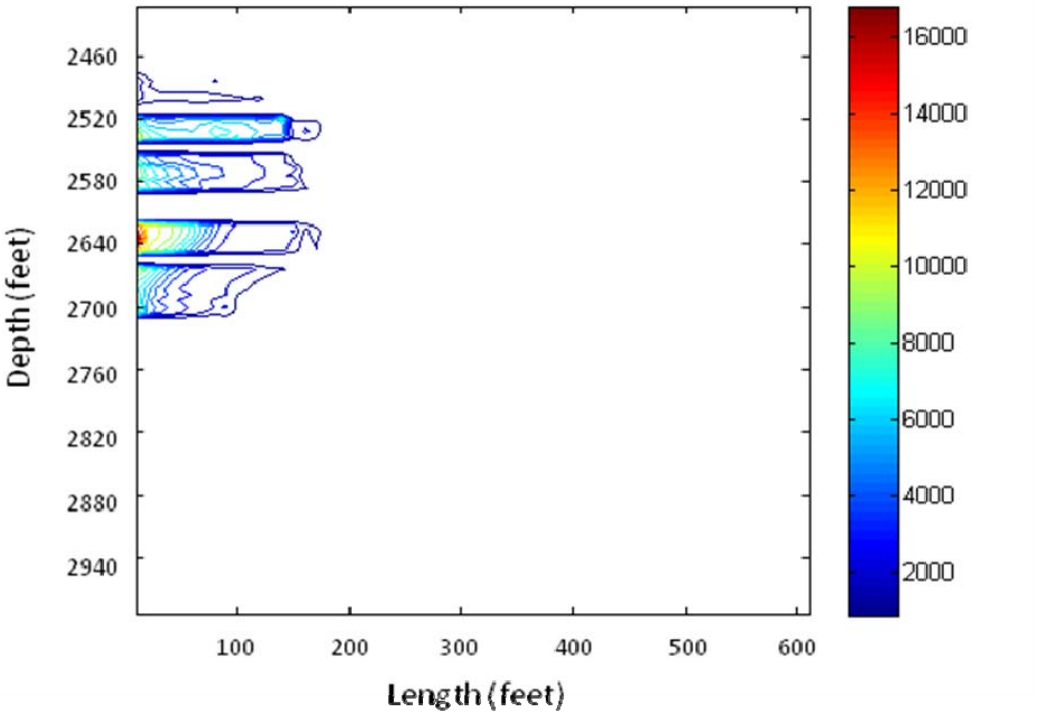

Fig. 4.3—Calculated Nierode-Kruk acid fracture conductivity contours (md-ft) at zero closure stress.

The shape of the conductivity contours at zero closure stress are similar to the E-StimPlan output for conductivity with closure stress and the acid etched width profile. At zero closure stress, the acid etched width solely determines the acid fracture conductivity in the Nierode and Kruk (1973) correlation.

The conductivity across each fracture stage can also be calculated using the Mou et al. (2010) conductivity correlations. The permeability distribution dominant case is applicable to this well. The derived geostatistical parameters vary between fracture stages and result in different conductivity contours for each stage (**Figs. 4.4-4.7**).

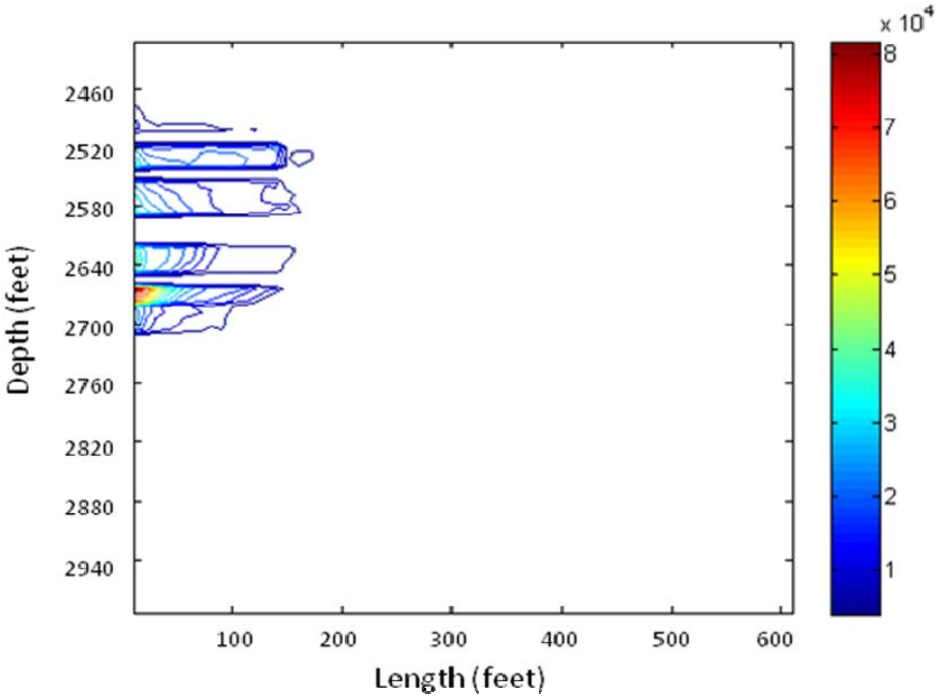

Fig. 4.4—Stage 1 fracture conductivity contours (md-ft).

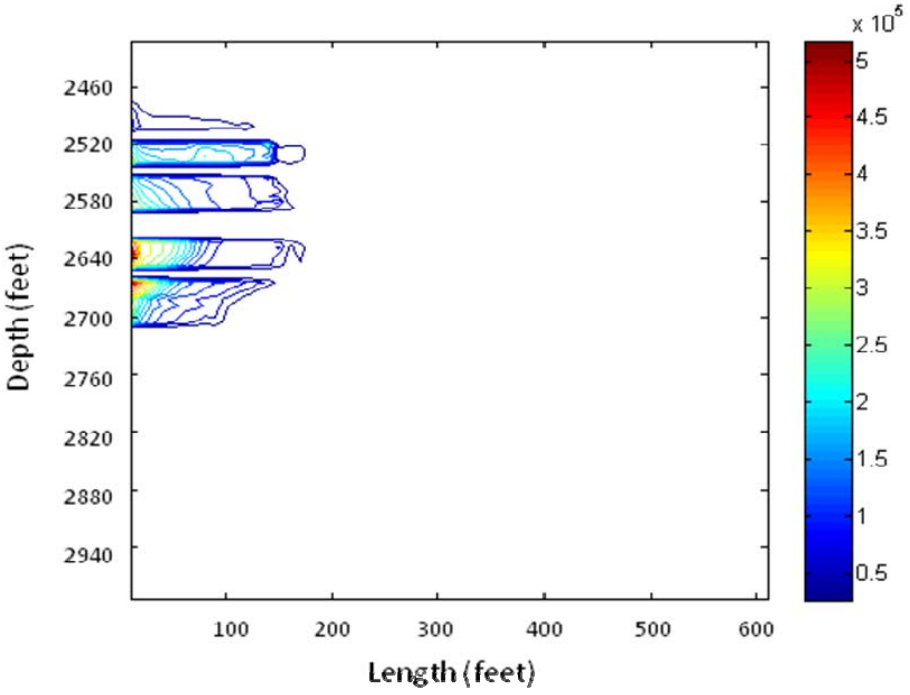

Fig. 4.5—Stage 2 fracture conductivity contours (md-ft).

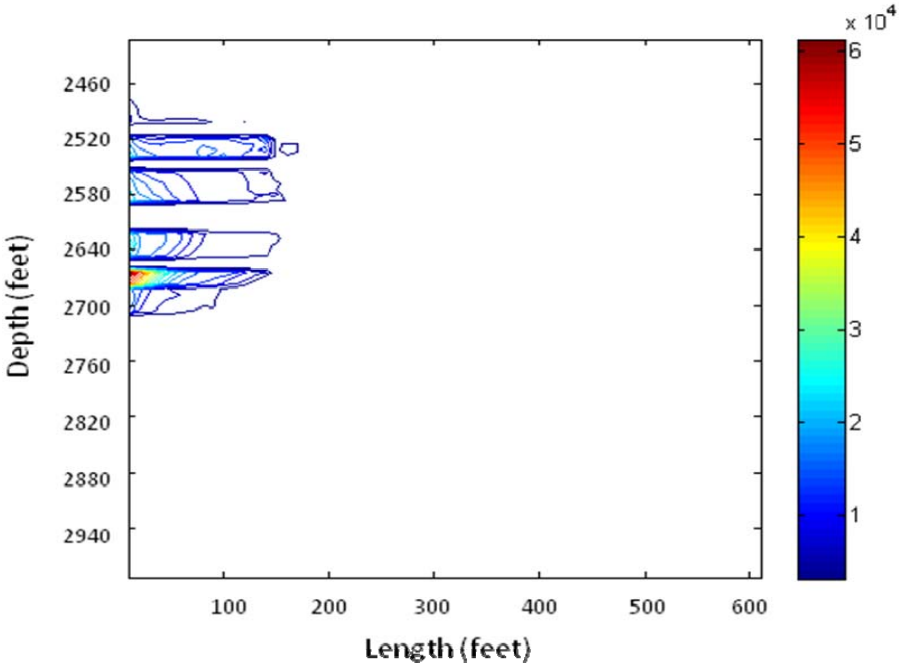

Fig. 4.6—Stage 3 fracture conductivity contours (md-ft).

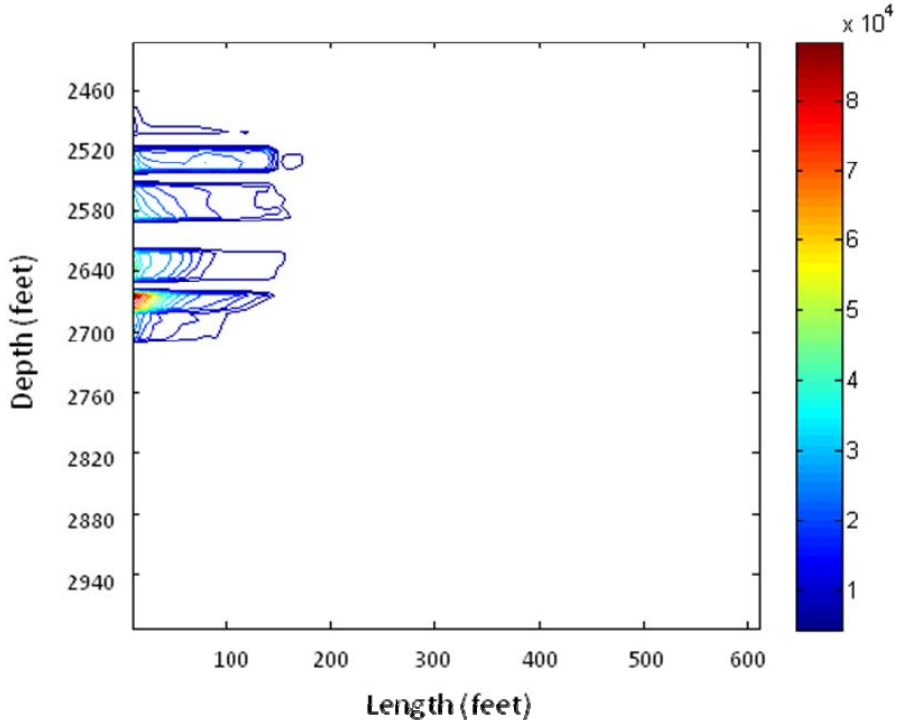

Fig. 4.7—Stage 4 fracture conductivity contours (md-ft).

The pattern of conductivity is based on etched width, which is the same across all stages. Therefore, the fracture conductivity contours display almost identical shape. However, the changing geostatistical parameters create order of magnitude differences in conductivity between fracture stages. The high horizontal correlation length and standard deviation of permeability along Stage 2 result in high conductivity using the Mou et al. (2010) correlations. Average conductivity is calculated with the method described in Economides et al. (1994). Note that the fluid loss Peclet number is greater than three. A summary of calculated average conductivity is presented in Table 4.1.

Table 4.1-Summary of average acid fracture conductivity.

	Average Fracture Conductivity (md-ft)
Nierode-Kruk (965 psi closure stress)	854
Nierode-Kruk (zero closure stress)	1,560
Stage 1	5,910
Stage 2	52,000
Stage 3	4,070
Stage 4	6,550

The method presented in Economides et al. (1994) for calculation of equivalent fracture skin is used, which relies on calculation of parameter F_{CD}:

$$F_{CD} = \frac{k_f w}{k x_f} \quad \text{.....(4.1)}$$

When parameter F_{CD} is greater than 10, the fracture is said to have infinite conductivity. Given the calculated average fracture conductivity for each case, infinite conductivity occurs using both the Mou et al. (2010) and Nierode-Kruk (1973) conductivity correlations. This results in an individual equivalent fracture skin of approximately -5.3.

5. CONCLUSION

5.1 Comparison of Conductivity Predictions

For the case in the Hugoton Field, the Nierode-Kruk conductivity correlation significantly underestimated the expected acid fracture conductivity when compared to the results using the Mou et al. (2010) conductivity correlations (**Fig. 5.1**).

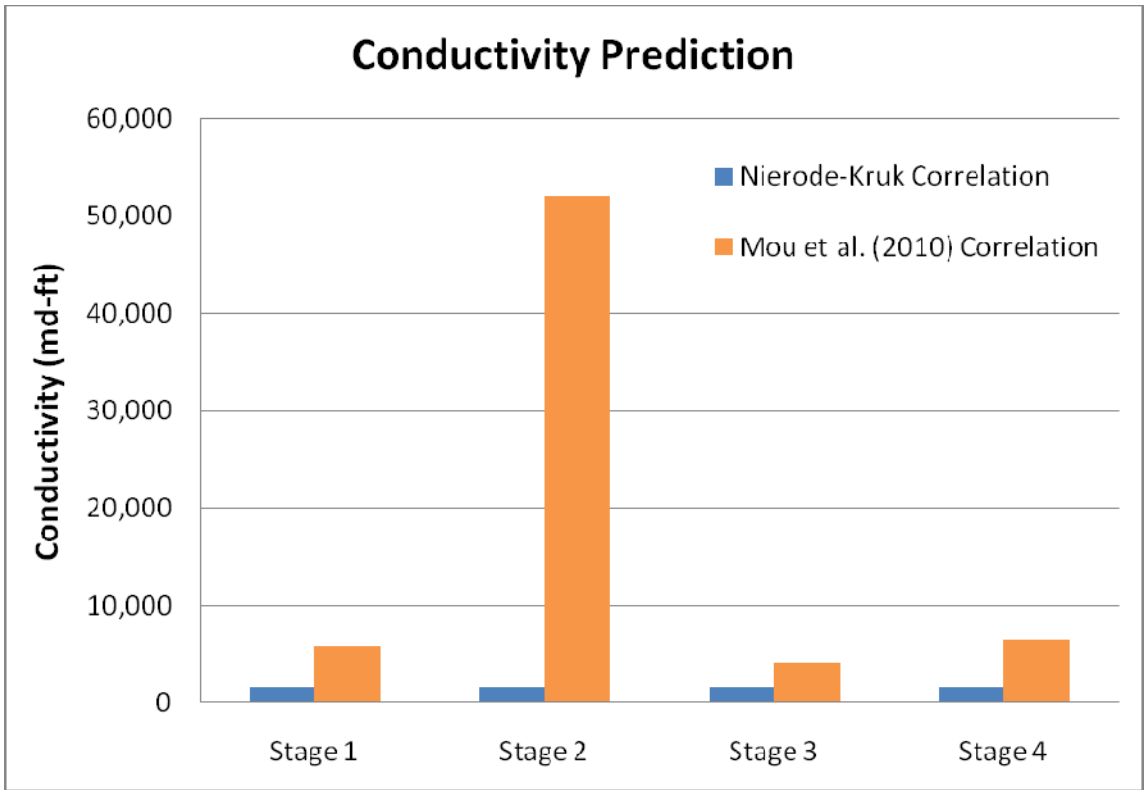

Fig. 5.1—Comparison of conductivity correlations at zero closure stress across four fracture stages.

The Nierode-Kruk conductivity correlation predicts equal conductivity for each fracture stage (rock embedment strength is assumed not to change along the lateral),

whereas the Mou et al. (2010) correlation results in a more realistic variation in conductivity based on changes in formation properties along the over 1,000 foot lateral. The Hugoton Field is laterally continuous, but small scale variation in petrophysical properties significantly affects resulting acid fracture conductivity. Differences in conductivity between stages are caused primarily by changes in the σ_D parameter, which controls surface roughness and local acid etched width. Increasing this parameter results in more surface unevenness and deep void spaces. Therefore, as σ_D increases acid fracture conductivity also increases, hence the dramatic increase in acid fracture conductivity along Stage 2.

Even though the conductivity varies between stages using the Mou et al. (2010) correlations, the conductivity predicted using these correlations is consistently higher than that predicted using the Nierode-Kruk correlation. This is again due to the lateral continuity of the field, which results in high $\lambda_{D,x}$ and low $\lambda_{D,z}$. During the acid fracture treatment, high-conductivity channels will be created that extend horizontally away from the wellbore and into the formation. The Mou (2009) model incorporates this behavior into the resulting correlations, but the Nierode-Kruk correlation has no term to capture this feature.

5.2 Future Work

The Mou et al. (2010) correlations were developed for grid blocks 10 feet by 10 feet in size. A maximum value of one was used for some dimensionless geostatistical parameters in calculation of the conductivity, even though the geostatistical features

extend past the realm of the 10 foot by 10 foot grid block. The Mou (2009) model needs to be upscaled if it is to capture precisely the impact of geostatistical features over an entire fracture. Applying the correlation across a fracture using individual grid blocks results in a broken view of how channels are created and sustained. These features may in reality extend over a hundred feet (e.g., Stage 4). Somehow the continuity of these features must be preserved across grid blocks besides just assuming a maximum dimensionless parameter. The upscaling procedure also needs to address the various scales of cyclicity observed across the variograms (e.g., Stage 1) as the Mou et al. (2010) correlations only reflect one scale based on the 10 foot by 10 foot gridding scheme. High permeability streaks as observed in the Well 2 Lower Fort Riley permeability dataset should also be preserved, which will require model conditioning. Future work will investigate a solution to these issues, incorporating the features of small scale heterogeneity into an acid fracture simulator that accurately models conductivity over the entire fracture.

REFERENCES

Ahr, W.M. 2008. *Geology of Carbonate Reservoirs*. Hoboken, New Jersey: John Wiley & Sons, Inc.

American Petroleum Institute (API). 1998. *Recommended practices for core analysis, second edition*. Washington, D.C.: API Publishing Services.

Antelo, L.F., Pournik, M., Zhu, D., and Hill, A.D. 2009. Surface Etching Pattern and its Effect on Fracture Conductivity in Acid Fracturing. Paper SPE 119743 presented at the SPE Hydraulic Fracturing Technology Conference, The Woodlands, Texas, 19-21 January.

Borgia, G.C., Bortolotti, V., Dattilo, P., and Fantazzini, P. 1997. Quantitative Determination of the Degree of Heterogeneity Within an Outcropping Reservoir by Magnetic Resonance Imaging. Paper SPE 38751 presented at the SPE Annual Technical Conference and Exhibition, San Antonio, Texas, 5-8 October.

Buchanan, R.C. and McCauley, J.R. 1987. *Roadside Kansas: A Traveler's Guide to Its Geology and Landmarks*. Lawrence, Kansas: University Press of Kansas.

Deng, J., Zhu, D., and Hill, A.D. 2009. A Theoretical Study of Acid Fracture Conductivity Under Closure Stress. Paper SPE 124755 presented at the SPE Annual Technical Conference and Exhibition, New Orleans, Louisiana, 4-7 October.

Dubois, M.K., Byrnes, A.P., Bohling, G.C., and Doveton, J.H. 2006. Multiscale geologic and petrophysical modeling of the giant Hugoton Gas Field (Permian), Kansas and Oklahoma, U.S.A. In *Giant Hydrocarbon Reservoirs of the World: From Rocks to Reservoir Characterization and Modeling*, eds. P.M. Harris and L.J. Weber, 307-353. Tulsa, Oklahoma: American Association of Petroleum Geologists and Society for Sedimentary Geology.

Ebbs Jr., D.J., Works, A.M., and Fetkovich, M.J. 1990. A Field Case Study of Replacement Well Analysis: Guymon-Hugoton Field, Oklahoma. Paper SPE 20755 presented at the SPE Annual Technical Conference and Exhibition, New Orleans, Louisiana, 23-26 September.

Economides, M.J., Hill, A. D., and Ehlig-Economides, C. 1994. *Petroleum Production Systems*. Upper Saddle River, New Jersey: Prentice Hall, Inc.

Gangi, A.F. 1978. Variation of whole and fractured porous rock permeability with confining pressure. *Int. J. Rock Mech. Min. Sci. Geomech. Abstr.* **15** (5): 249-257.

Goggin, D.J., Chandler, M.A., Kocurek, G., and Lake, L.W. 1988. Patterns of Permeability in eolian deposits: Page Sandstone (Jurassic), northeastern Arizona. *SPE Form. Eval.* **3** (2): 297-306.

Goggin, D.J., Chandler, M.A., Kocurek, G., and Lake, L.W. 1992. Permeability transects of eolian sands and their use in generating random permeability fields. *SPE Form. Eval.* **7** (1): 7-16.

Gong, M., Lacote, S., and Hill, A.D. 1998. New Model of Acid-Fracture Conductivity Based on Deformation of Surface Asperities. Paper SPE 57017 presented at the SPE International Formation Damage Symposium, Lafayette, Louisiana, 18-19 February.

Gringarten, E. and Deutsch, C.V. 1999. Methodology for Variogram Interpretation and Modeling for Improved Reservoir Characterization. Paper SPE 56654 presented at the SPE Annual Technical Conference and Exhibition, Houston, Texas, 3-6 October.

Hartkamp-Bakker, C.A. and Donselaar, M.E. 1993. Permeability patterns in point bar deposits: Tertiary Loranca Basin, Central Spain. In *The Geological Modelling of Hydrocarbon Reservoirs and Outcrop Analogues*, eds. S.S. Flint and I.D. Bryant, 157-168. Cambridge, Massachusetts: The International Association of Sedimentologists and Blackwell Scientific Publications.

Isaaks, E.H. and Srivastava, R.M. 1989. *An Introduction to Applied Geostatistics*. New York: Oxford University Press, Inc.

Jennings Jr., J.W., Ruppel, S.C., and Ward, W.B. 1998. Geostatistical Analysis of Petrophysical Data and Modeling of Fluid-Flow Effects in Carbonate Outcrops. Paper SPE 49025 presented at the SPE Annual Technical Conference and Exhibition, New Orleans, Louisiana, 27-30 September.

Jones, S.C. 1992. A New, Fast, Accurate Pressure-Decay Probe Permeameter. Paper SPE 24757 presented at the SPE Annual Technical Conference and Exhibition, Washington, D.C., 4-7 October.

LeFever, R.B. and Schaefer, H. 1947. Productivity of Individual Pay Zones Used for Determining Completion Efficiences – Hugoton Field, Kansas. Paper API 47-133 presented at the Mid Continent District spring meeting, Division of Production, Amarillo, Texas, 27 May.

Lisigurski, O. and Rowe, G.C. 2006. Practical Steps To Increase Production and Reserves in Mature Gas Fields: Hugoton and Panoma, Texas County, Oklahoma, U.S.A. Paper SPE 102259 presented at the SPE Annual Technical Conference and Exhibition, San Antonio, Texas, 24-27 September.

Malagon, C., Pournik, M., and Hill, A.D. 2006. The Texture of Acidized Fracture Surfaces – Implications for Acid Fracture Conductivity. Paper SPE 102167 presented at the SPE Annual Technical Conference and Exhibition, San Antonio, Texas, 24-27 September.

Mazzullo, S.J., Teal, C.S., and Burtnett, C.A. 1996. *Chase Group Strata in North-Central Kansas and Nebraska: Outcrop Analogs of Stratigraphic-Trap Reservoirs*. Wichita, Kansas: Kansas Geological Society.

Mazzullo, S.J. 1998. Stratigraphic architecture of lower Permian cyclic carbonate reservoirs (Chase Group) in the mid-continent USA, based on outcrop studies. *AAPG Bulletin* **82** (3): 464-483.

Mazzullo, S.J. 1999. Road Log and Locality Guide: The Chase Group in Southern Kansas: Lithostratigraphy, Facies, and Sequence Stratigraphic Architecture. Paper presented at the Midcontinent AAPG Meeting, Wichita, Kansas, 29-31 August.

Mou, J. 2009. Modeling acid transport and non-uniform etching in a stochastic domain in acid fracturing. PhD dissertation, College Station: Texas A&M University.

Mou, J., Zhu, D., and Hill, A.D. 2009. Acid-Etched Channels in Heterogeneous Carbonates–A Newly Discovered Mechanism for Creating Acid Fracture Conductivity. Paper SPE 119619 presented at the SPE Hydraulic Fracturing Technology Conference, The Woodlands, Texas, 19-21 January.

Mou, J., Zhu, D., and Hill, A.D. 2010. New Correlations of Acid Fracture Conductivity at Low Closure Stress Based on the Spatial Distributions of Formation Properties. Paper SPE 131591 presented at the CPS/SPE International Oil & Gas Conference and Exhibition, Beijing, China, 8-10 June.

Nierode, D.E. and Kruk, K.F. 1973. An Evaluation of Acid Fluid Loss Additives, Retarded Acids, and Acidized Fracture Conductivity. Paper SPE 4549 presented at the SPE Annual Fall Meeting, Las Vegas, Nevada, 30 September – 3 October.

Pournik, M., Zhu, D., and Hill, A.D. 2009. Acid-Fracture Conductivity Correlation Development Based on Acid-Fracture Characterization. Paper SPE 122333 presented at the SPE European Formation Damage Conference, Scheveningen, The Netherlands, 27-29 May.

Pranter, M.J., Hirstius, C.B., and Budd, D.A. 2005. Scales of lateral petrophysical heterogeneity in dolomite lithofacies as determined from outcrop analogs: Implications for 3-D reservoir modeling. *AAPG Bulletin* **89** (5): 645-662.

Remy, N., Boucher, A., Wu, J., and Li, T. 2008. *SGeMS: Stanford Geostatistical Modeling Software Version 2.1* [computer software]. Palo Alto, California: Board of Trustees of Stanford University.

Ruffet, C.S., Fery, J.J., and Onaisi, A. 1997. Acid-Fracturing Treatment: A Surface-Topography Analysis of Acid-Etched Fractures to Determine Residual Conductivity. Paper SPE 38175 presented at the SPE European Formation Damage Conference, The Hague, The Netherlands, 2-3 June.

Siemers, W.T. and Ahr, W.M. 1990. Reservoir Facies, Pore Characteristics, and Flow Units: Lower Permian Chase Group, Guymon-Hugoton Field, Oklahoma. Paper SPE 20757 presented at the SPE Annual Technical Conference and Exhibition, New Orleans, Louisiana, 23-26 September.

Smith, M.B. 2008. *StimPlan™/InjecPlan™ Version 6.00* [computer software]. Tulsa, Oklahoma: NSI Technologies, Inc.

Tomutsa, L., Jackson, S.R., and Szpakiewicz, M. 1986. Geostatistical Characterization and Comparison of Outcrop and Subsurface Facies: Shannon Shelf Sand Ridges. Paper SPE 15127 presented at the SPE California Regional Meeting, Oakland, California, 2-4 April.

Walsh, J.B. 1981. Effect of pore pressure and confining pressure on fracture permeability. *Int. J. Rock Mech. Min. Sci. Geomech. Abstr.* **18** (5), 429-435.

VITA

Cassandra Vonne Beatty received her Bachelor of Science degree in biological engineering from Cornell University in 2007. She entered the Department of Petroleum Engineering at Texas A&M University in January 2009 and was awarded a Master of Science degree in August 2010. Her research interests include geologic characterization, carbonates, and stimulation technologies. She plans to continue work on acid fracture conductivity prediction as a Ph.D. candidate in September 2010 in the Department of Petroleum Engineering at Texas A&M University.

Ms. Beatty may be reached at the Department of Petroleum Engineering, Texas A&M University, 3116 TAMU – 714 Richardson Building, College Station, TX 77843-3116. Her email is cassandra.beatty@pe.tamu.edu.